Small molecule cognitive enhancer reverses age-related memory decline in mice.

SHORT TITLE: Reversing aging related deficits

Authors: Karen Krukowski[1,2], Amber Nolan[2,3,*], Elma S. Frias[1,2,*], Morgane Boone[4*,] Gonzalo Ureta[5], Katherine Grue[1,2], Maria-Serena Paladini[1,2], Edward Elizarraras[1,2], Luz Delgado[5], Sebastian Bernales[5], Peter Walter[4,6] and Susanna Rosi[1,2,7,8,9]

[1] Department of Physical Therapy and Rehabilitation Science, University of California at San Francisco, San Francisco, CA, USA.
[2] Brain and Spinal Injury Center, University of California at San Francisco, San Francisco, CA, USA.
[3] Department of Pathology, University of California at San Francisco, San Francisco, CA, USA.
[4] Biochemistry and Biophysics, University of California at San Francisco, San Francisco CA, USA.
[5] Fundación Ciencia & Vida, Santiago, Chile.
[6] Howard Hughes Medical Institute, University of California at San Francisco, San Francisco, CA, USA.
[7] Department of Neurological Surgery, University of California at San Francisco, San Francisco, CA, USA.
[8] Weill Institute for Neuroscience, University of California at San Francisco, San Francisco, CA, USA.
[9] Kavli Institute of Fundamental Neuroscience, University of California at San Francisco, San Francisco, CA, USA.

*authors contributed equally

<u>Corresponding Authors:</u>

Susanna Rosi, Ph.D. Lewis and Ruth Cozen Chair II
Professor
1001 Potrero Ave,
Zuckerberg San Francisco General Hospital
Building #1 Room 101
San Francisco, CA 94110
Tel.: +1-415-206-3708
Email: susanna.rosi@ucsf.edu

Peter Walter, PhD, Professor
Box 2200, UCSF
San Francisco, CA 94143
Phone: +1-415-476-5017
Email: peter@walterlab.ucsf.edu

1

45 **ONE SENTENCE SUMMARY**
46 Inhibition of the integrated stress response restores neuronal and immune dysfunction
47 and alleviates memory deficits in aged mice.
48

49 **ABSTRACT**

50 With increased life expectancy age-associated cognitive decline becomes a growing

51 concern, even in the absence of recognizable neurodegenerative disease. The

52 integrated stress response (ISR) is activated during aging and contributes to age-

53 related brain phenotypes. We demonstrate that treatment with the drug-like small-

54 molecule ISR inhibitor ISRIB reverses ISR activation in the brain, as indicated by

55 decreased levels of activating transcription factor 4 (ATF4) and phosphorylated

56 eukaryotic translation initiation factor eIF2. Furthermore, ISRIB treatment reverses

57 spatial memory deficits and ameliorates working memory in old mice. At the cellular

58 level in the hippocampus, ISR inhibition i) rescues intrinsic neuronal electrophysiological

59 properties, ii) restores spine density and iii) reduces immune profiles, specifically

60 interferon and T cell-mediated responses. Thus, pharmacological interference with the

61 ISR emerges as a promising intervention strategy for combating age-related cognitive

62 decline in otherwise healthy individuals.

63

64 **INTRODUCTION**

65

66 "Of the capacities that people hope will remain intact as they get older, perhaps the

67 most treasured is to stay mentally sharp" (*1*).

68

69 The impact of age on cognitive performance represents an important quality-of-life and

70 societal concern, especially given our prolonged life expectancy. While often discussed

71 in the context of disease, decreases in executive function as well as learning and

72 memory decrements in older, healthy individuals are common (*2, 3, 4 , 5*). According to

73   the US Department of Commerce the aging population is estimated by 2050 to reach

74   83.7 million individuals above 65 years of age in the US; this represents a rapidly

75   growing healthcare and economic concern (*6*).

76

77   Age-related decline in memory has been recapitulated in preclinical studies with old

78   rodents (*7-10*). Specifically, prior studies have identified deficits in spatial memory (*9,*

79   *11*), working and episodic memory (*8, 10*) and recognition memory (*12*), when

80   comparing young, adult mice with older sex-matched animals. The hippocampus is the

81   brain region associated with learning and memory formation and is particularly

82   vulnerable to age-related changes in humans and rodents (*13-16*). Deficits in a number

83   of cellular processes have been suggested as underlying causes based on correlative

84   evidence, including protein synthesis (*17*), metabolism (*18*), inflammation (*19*), and

85   immune responses (*9, 11, 20, 21*). While providing a wealth of parameters to assess, by

86   and large the causal molecular underpinnings of age-related memory decline have

87   remained unclear.

88

89   The principle that blocking protein synthesis prevents long-term memory storage was

90   discovered many years ago (*22*). With age there is a marked decline of protein

91   synthesis in the brain that correlates with defects in proper protein folding (*12, 23-25*)**.**

92   Accumulation of misfolded proteins can activate the integrated stress response (ISR)

93   (*26*), an evolutionary conserved pathway that decreases protein synthesis. In this way,

94   the ISR may have a causative role in age-related cognitive decline. We previously

95   discovered that interference with the drug-like small-molecule inhibitor (integrated stress

96 response inhibitor, or ISRIB) rescued traumatic brain injury-induced behavioral and

97 cognitive deficits (*27-29*), suggesting that this pharmacological tool may be useful in

98 testing this notion.

99

100 Increasing age leads to structural and functional changes in hippocampal neurons.

101 Specifically, in old animals there is an increase in neuronal hyperpolarization after

102 spiking activity ("afterhyperpolarization", or AHP) that decreases intrinsic neuronal

103 excitability and correlates with memory deficits (*13-16, 30*). Aging also manifests itself

104 with synaptic excitability changes in the hippocampus that correlate with a reduction in

105 the bulbous membrane projections that form the postsynaptic specializations of

106 excitatory synapses, termed dendritic spines (*31, 32*). Morphological changes in

107 dendritic spine density are critical for spatial learning and memory (*33, 34*). Whether

108 these age-related neuronal changes can be modified or are linked with ISR activation

109 has yet to be determined.

110

111 In addition to neuronal changes, ISR activation can modify immune responses via

112 alterations in cytokine production (*35*). Indeed, maladaptive immune responses have

113 been linked with cognitive decline in the old brain (*8, 9, 11, 20*). Initial studies focused

114 on age-associated cytokine responses, including interferon (IFN)-mediated cognitive

115 changes (*20, 36*). Type-I IFN responses can induce age-related phenotypes in rodents.

116 Furthermore, the adaptive immune system (T cell infiltration into the old brain) can

117 regulate neuronal function via IFN-γ production (*21*), suggesting the possibility that age-

118 induced maladaptive immune responses and the ISR are linked. Here we explore the

119 possibility of ISR inhibition by ISRIB as a potential strategy for modifying age-induced

120 neuronal, immune, and cognitive dysfunction.

121

122

123 **RESULTS**

124

125 *ISRIB resets the ISR in the brain of old mice.*

126

127 ISR activation leads to global reduction in protein synthesis but also to translational up-

128 regulation of a select subset of mRNAs whose translation is controlled by small

129 upstream open-reading frames in their 5'-UTRs (*37, 38*). One well-studied ISR-

130 upregulated target protein is ATF4 (activating transcription factor 4) (*39, 40*). We

131 recently showed ISRIB administration reversed mild head trauma-induced elevation in

132 ATF4 protein (*28*). Using the same ISRIB treatment paradigm of daily injections on 3

133 consecutive days (*27, 28*), we found decreased age-associated ATF4 protein levels in

134 mouse brain lysates when compared to vehicle-treated controls during ISRIB

135 administration (Figure 1 -**Supplemental Figure 1**). ATF4 levels 18 days after cessation

136 of ISRIB treatment showed persistent reduction in age-induced ATF4 protein levels that

137 were indistinguishable from young mice (**Figure 1A**, **B**, Figure 1 **- Supplemental**

138 **Figure 2A**).

139

140 The key regulatory step in the ISR lies in the phosphorylation of eukaryotic translation

141 initiation factor eIF2 (*26*). Four known kinases can phosphorylate Ser51 in its α-subunit

142 of (eIF2α) to activate the ISR (*41*): HRI (heme-regulated inhibitor), PKR (double-

143 stranded RNA-dependent protein kinase), PERK (PKR-like ER kinase) and GCN2

144 (General amino acid control nonderepressible 2). Only three of these kinases are known

145 to be expressed in the mammalian brain (PKR, PERK, GCN2). To understand upstream

146 modifiers of age-related ISR activation, we investigated the impact of age and ISRIB

147 administration on the expression of these kinases. We found a modest, but significant

148 increase in activated GCN2 (as indicated by its phosphorylated form p-GCN2) when

149 comparing young and old brain lysates (**Figure 1C**, Figure 1 - **Supplemental Figure**

150 **2B**). Moreover, when ISRIB was administered weeks prior (**Figure 1A**), GCN2

151 activation returned to levels comparable to young brains (**Figure 1C**, Figure 1 -

152 **Supplemental Figure 2B**). Age and ISRIB did not impact phosphorylation status of

153 PERK and PKR in total brain lysates (**Figure 1D**,**E**, Figure 1 - **Supplemental Figure**

154 **2B**). Thus, brief ISRIB administration in the old brain has long-lasting effects on ISR

155 activation.

156

157 *Inhibition of the ISR reverses age-induced decline in spatial learning and memory.*

158

159 To assess whether the reduction in ISR activation affects age-related cognitive defects,

160 we tested the capacity for spatial learning and memory in young and old mice in a radial

161 arm water maze (*27, 42*). This particular forced-swim behavior tool measures

162 hippocampal-dependent spatial memory functions in rodents and has been previously

163 used to assess age-related cognitive deficits (*7, 43*). Animals were trained for two days

164 (two learning blocks/day) to locate a platform hidden under opaque water in one of the

165 eight arms using navigational cues set in the room (**Figure 2A**). We recorded the total

166 number of entries into the non-target arm (errors) before the animal found the escape

167 platform with automated tracking software and used it as a metric of learning. After two

168 days of training, young animals averaged one error prior to successfully locating the

169 escape platform, while old animals averaged three errors, indicating their reduced

170 learning capacity (Figure 2 - **Supplemental Figure 1A**).

171

172 We next tested whether pharmacological inhibition of the ISR could modify the age-

173 related spatial learning deficits. ISRIB treatment started the day before the first training

174 day and continued with daily injections throughout the duration of the training (3

175 injections in total; see **Figure 2A**, left). By the end of two days of training, ISRIB-treated

176 old animals averaged two errors prior to finding the escape platform, while vehicle-

177 treated old animals averaged three, denoting significant learning improvement in the

178 mice that received ISRIB (Figure 2 - **Supplemental Figure 1B**). No difference in

179 learning performance was measured in young mice that received the identical treatment

180 paradigm (Figure 2 - **Supplemental Figure 1C**), suggesting that ISRIB-induced

181 learning improvement measured in this training regime is age-dependent. These results

182 were confirmed in an independent old animal cohort, in which we tested an additional

183 ISR inhibitor (Cmp-003, a small molecule with improved solubility and pharmacological

184 properties (PCT/US18/65555)), using an identical training/injection paradigm (Figure 2 -

185 **Supplemental Figure 1D**). Old animals that received Cmp-003 made significantly fewer

186 errors prior to locating the escape platform than old animals that received vehicle

187 injections, again indicating significant learning improvement.

188

Spatial memory of the escape location was measured one week later by reintroducing the animals into the pool and measuring the number of errors before they located the hidden platform. The animals did not receive any additional treatment during this task. Old mice treated with ISRIB one week before made significantly fewer errors compared to matched, vehicle-treated old male (**Figure 2B**) and female (Figure 2 - **Supplemental Figure 2**) mice. Remarkably, the memory performance of old animals treated with ISRIB a week before was comparable to that of young mice (**Figure 2B**). These results demonstrate that brief treatment with ISRIB rescues age-induced spatial learning and memory deficits, cementing a causative role of the ISR on long-term memory dysfunction .

ISRIB administration improves age-induced deficits in working and episodic memory weeks after treatment.

Given the long-lasting effect of brief ISRIB treatment on ATF4 protein levels in the brain and on memory function one week after drug administration, we next tested the duration of ISRIB effects on age-related cognitive function. On experimental day 20 (18 days post ISRIB treatment, **Figure 2A**, right), we measured working and episodic memory using a delayed-matching-to-place paradigm (DMP) (*27, 44*) in the same animal cohort without additional ISRIB treatment. Previous work has demonstrated that old mice display significant impairments when compared to young mice (*8, 10*). During DMP

211 animals learned to locate an escape tunnel attached to one of 40 holes in a circular

212 table using visual cues. The escape location was changed daily, forcing the animal to

213 relearn its location. To quantify performance, we used analysis tracking software to

214 measure "escape latency", reporting the time taken by the mouse to enter the escape

215 tunnel.

216

217 Old mice that received ISRIB treatment 18 days earlier displayed significant

218 improvement over the four-day testing period (**Figure 2C**; Day 20 vs. Day 23). By Day

219 23 post-treatment animals were locating the escape tunnel on average 20 seconds

220 faster than the matched-vehicle group (**Figure 2C**). This behavior is indicative of

221 improved working and episodic memory. By contrast, old animals that received vehicle

222 injections did not learn the task (**Figure 2C**; Day 20 vs. Day 23), as previously observed

223 (*8, 10*). These results demonstrate that ISRIB administration increases cognitive

224 performance in a behavioral paradigm measured weeks after administration.

225

226 *ISRIB treatment reverses age-associated changes in hippocampal neuron function.*

227

228 To determine the neurophysiological correlates of ISRIB treatment on cognition, we

229 investigated its effects on hippocampal neuronal function. Utilizing whole cell patch

230 clamping, we recorded intrinsic electrophysiological firing properties and synaptic input

231 in CA1 pyramidal neurons of young and old mice and compared them to those of old

232 mice treated with a single injection of ISRIB the day prior to recording (**Figure 3A**).

233

234 We evaluated alterations in intrinsic excitability by measuring action potential shape and

235 frequency properties and passive membrane response properties produced by a series

236 of hyperpolarizing and depolarizing current steps (20 steps from -250 to 700 pA, 250 ms

237 duration). We also assessed the hyperpolarization of the membrane potential following

238 high frequency firing, specifically the AHP following ~50 Hz spiking activity induced with

239 a current step (**Figure 3A**). In agreement with previous reports (*13-16, 30*), old mice

240 displayed a significantly increased AHP amplitude when compared to young mice

241 (**Figure 3B**). ISRIB treatment reversed the age-induced increase in AHP amplitude,

242 rendering the CA1 neuronal response in ISRIB-treated old mice indistinguishable from

243 young mice (**Figure 3B**). We did not find significant differences in other action potential

244 or passive membrane properties between groups (Figure 3 - **Supplemental Figure 1**).

245

246 We also measured spontaneous excitatory postsynaptic currents (sEPSC), while

247 holding the cell at -75 mV in a voltage clamp. Both the frequency and amplitude of

248 sEPSCs were indistinguishable between groups (Figure 3 - **Supplemental Figure 2**).

249 These data support that ISRIB treatment in old animals restores neuronal function to

250 levels comparable to young neurons by affecting intrinsic excitability and specifically

251 reducing the AHP following high frequency firing.

252

253 *ISRIB treatment reduces dendritic spine loss.*

254

255 To determine if ISRIB might affect age-induced synaptic structural changes, we

256 quantified dendritic spine density after ISRIB treatment in old mice with fluorescently

257 labeled excitatory neurons (marked by a genomically encoded Thy1-YFP fusion

258 protein). The hippocampus of old mice is characterized by a reduction in dendritic spine

259 density that correlates with diminished cognitive output (*31, 32*). Old Thy1-YFP

260 expressing mice received ISRIB treatment and two days of behavioral training as

261 described in **Figure 2A**. At the end of Day 2, we terminated the animals and harvested

262 the brains for quantification of dendritic spine density in the hippocampus (stratum

263 radiatum of CA1) (**Figure 3C**) using confocal microscopy imaging and unbiased

264 analysis (**Figure 3D**). Similar to previous reports, we measured a significant reduction in

265 dendritic spine density in old when compared to young Thy1-YFP mice (**Figure 3E**) (*31,*

266 *32*). ISRIB treatment significantly increased spine numbers when compared with age-

267 matched vehicle-treated mice (**Figure 3E**). Taken together these data demonstrate that

268 ISRIB administration improves both neuron structure and function in old mice.

269

270 *Age-induced inflammatory tone is reduced following ISRIB treatment.*

271

272 Because it is known that immune dysregulation in the brain increases with age (*45*) and

273 correlates with reduced cognitive performance in old animals (*8, 9, 11, 20*), we next

274 investigated immune parameters impacted by ISRIB administration in the old brain. To

275 this end, we first investigated glial cell activation (microglia and astrocytes) in

276 hippocampal sections from of old mice and ISRIB-treated old mice by fluorescent

277 microscopic imaging (during ISRIB administration, Figure 4 - **Supplemental Figure 1**).

278 We measured, astrocyte and microglia reactivity as the percent area covered by GFAP

279 and Iba-1. In these analyses, we observed no differences between the old and ISRIB-

280 treated old animals (Figure 4 - **Supplemental Figure 1B-G**).

281

Next, we performed quantitative PCR (qPCR) analyses on hippocampi from young, old, and ISRIB-treated animals on samples taken at the same time point as in the microscopic analysis (Figure 4 - **Supplemental Figure 1A**). We measured a panel of inflammatory markers, many of which are known to increase with age (*45*), with a particular focus on IFN-related genes as this pathway is implicated in age-related cognitive decline (*20, 36*). Indeed, we found that age increased expression of a number of IFN response pathway genes, *Rtp4, Ifit1, and Gbp10* (**Figure 4A**-**C**). Importantly, ISRIB administration reduced expression of *Rtp4, Ifit1, and Gbp10* to levels that became indistinguishable from young animals (**Figure 4A-C**). Other inflammatory makers were also increased with age (*Ccl2, Il6*) but not affected by ISRIB treatment, whereas *Cd11b* was increased upon ISRIB administration alone (**Table 1**).

293

Using these same hippocampal extracts, we next measured T cell responses. Similar to other reports (*21, 46*), we observed a significant increase in T cell marker mRNA expression (*Cd3*) in the hippocampus of old compared to young mice (**Figure 4D**). ISRIB treatment in the old mice reduced the expression of the T cell marker to a level comparable to that observed in young mice (**Figure 4D**). The ISRIB-induced reduction in T cell marker levels was not limited to the brain but extended to the peripheral blood of old animals, with CD8$^+$ T cell percentages reduced following ISRIB administration (**Figure 4E**). By contrast, we observed no changes in CD4$^+$ T cell levels (**Figure 4F**).

302

303 Given the broad and varied response of immune parameters in response to ISRIB

304 treatment, we next explored possible relationships between behavioral performance and

305 age-related inflammatory tone. T cell marker mRNA expression in the brain positively

306 correlated with cognitive performance: mice with lower T cell marker expression made

307 fewer errors prior to locating the escape platform during memory testing on Day 2

308 (**Figure 4G**). We also observed significant positive correlations when comparing

309 memory performance on day 2 (errors) with the mRNA levels of multiple IFN response

310 pathway genes (*Ifit1, Rtp4, Gbp10, Gbp5, Oasl1*) and additional inflammatory markers

311 (*Ccl2, Il6*) (**Figure 4G**). These data demonstrate that increased inflammatory marker

312 expression correspond with poorer cognitive performance, even when we did not

313 observed differences between the groups. These studies revealed that ISRIB treatment

314 impacts a broad number of immune parameters both in the periphery and in the brain

315 reducing the age-related inflammatory tone which strongly correlates with improved

316 cognition.

317

318 *ISRIB treatment resets age-related ISR activation*

319

320 Finally, we investigated the transcriptional expression of ISR mediators and neuronal

321 health markers in the hippocampal lysates used above. We did not detect differences in

322 *Gadd34 (Ppp1r15a) , Pkr (Eif2ak2), Bdnf1,* and *Ophn1* mRNA levels with age or ISRIB

323 treatment (**Table 1**). Interestingly however, when analyzed as individual animals, we

324 found a negative correlation between *Ppp1r15a* mRNA and cognitive performance:

325 animals with less *Ppp1r15a* mRNA made more errors prior to locating the escape

326 platform during memory testing (**Figure 5A**). GADD34, the regulatory subunit of one of

327 the two eIF2α phosphatases, acts in a feedback loop as a downstream target of ATF4

328 (*47-49*). Induction of GADD34 leads to decreased phosphorylation of eIF2 which

329 counteracts ISR activation. Indeed, ISRIB treatment reduced p-eIF2 levels in total brain

330 lysates (**Figure 5B;** Figure 5 - **Supplemental Figure 1**), suggesting that ISRIB may

331 break a feedback loop thereby resetting age-related ISR activation.

332

333

334 **DISCUSSION**

335 Here we provide evidence for a direct involvement of the ISR in age-related cognitive

336 decline. Temporary treatment with ISRIB causes a long lasting down-regulation of ATF4

337 (measured up to 20 days post treatment). The "ISR reset" leads to improvement in

338 spatial, working, and episodic memory. At a cellular level the cognitive enhancement is

339 paralleled by i) improved intrinsic neuron excitability, ii) increased dendritic spine

340 density, iii) reversal of age-induced changes in IFN and T cell responses in the

341 hippocampus and blood, and iv) reversal of ISR activation. Thus, we identify broad-

342 spectrum anatomical, cellular, and functional changes caused by ISR activation in old

343 animals. If these findings in mice translate into human physiology, they offer hope and a

344 tangible strategy to sustain cognitive ability as we age.

345

346 Alterations in proteostasis, the process of protein synthesis, folding and degradation, is

347 a hallmark of aging (*23*). Accumulation of protein aggregate in the brain is a contributing

348 factor to disease development and progression in several age-related

349 neurodegenerative diseases including Alzheimer's and Parkinson's disease (*50, 51*).

350 The rate of protein synthesis reportedly also declines with age in various regions of the

351 brain (*17*). Protein synthesis is critical for memory consolidation and the ISR pathway is

352 one of the major nodes for protein synthesis control. Therefore, we investigated how

353 interference with the ISR impacted healthy age-related cognitive decline. ISRIB rapidly

354 enters the brain of old animals and interferes with ISR activation as measured by

355 decreased phosphorylation of eIF2α and ATF4 levels. ISRIB acts downstream of

356 phosphorylation of eIF2α (*52*); therefore the decrease in phosphorylation of eIF2α

357 suggests a possible block in the feedback loop that keeps the ISR activated in the old

358 brain; further investigation is needed to understand the exact mechanism. Initial findings

359 suggest this could be through modulation of the kinase GCN2. Here we found that age

360 increased activation of GCN2 (denoted by increased phosphorylation) was attenuated

361 by ISRIB administration. These data indicate that even brief inhibition of the ISR allows

362 the system to 'reset' and dampen the stress response in the old brain.

363

364 Along with the ISR, the mammalian target of rapamycin (mTOR), is the other important

365 pathway that cells employ to respond to environmental stress and balance between

366 survival and death.   Rapamycin, arguably the most studied and validated small

367 molecule for lifespan expansion, targets mTOR and therefore inhibits mTOR-controlled

368 mRNA translation. However, increased protein production due to mTOR (over)activation

369 can in turn induce the ISR (*53-55*), which serves as a governor keeping protein

370 synthesis in check. Interestingly, despite these two pathways regulating distinct stress

371 responses to translational regulation, it was recently reported that both the ISR and

372   mTOR converge at the level of mRNA translation and both inhibit the translation of the

373   same set of proteins (*56*). This complex interplay between mTOR signaling and the ISR

374   could potentially explain how pharmacological treatment with seemingly opposing

375   strategies could both be beneficial.

376

377   The reduction in ISR activation corresponded with improved memory performance in old

378   mice weeks after treatment was stopped. Importantly, brief ISRIB treatment improved

379   performance in two different behavioral paradigms (radial arm water maze and the

380   delayed matching to place) previously shown to capture age-related cognitive decline

381   (*8, 10, 11, 36, 43, 57*). These behavioral paradigms model different aspects of cognitive

382   loss observed during aging in rodents: spatial, working, and episodic memory (*42, 44*).

383   Therefore, our results suggest that ISR inhibition can reverse a broad spectrum of

384   cognitive decline. Notably, spatial learning reversal occurred during ISRIB treatment

385   while the effects on memory were measured weeks after administration and

386   demonstrate the long lasting effects of ISRIB even in the aging brain. Most of the

387   previous studies were performed exclusively in male rodents (*11, 36, 43, 57*). Sex-

388   dimorphic cognitive decline has been reported with age in humans (*58-60*) and rodents

389   (*61, 62*). In the current study we identified cognitive reversal with ISRIB administration in

390   both male and female mice; taking the critical first steps towards studying sex-dimorphic

391   age responses in the ISR. However, we only validated ISRIB-mediated neuronal and

392   immune correlates in male mice. Further work is required to investigate the restorative

393   effects in females.

394

395   The neuronal correlates of improved memory function were identified in measures of i)

396   intrinsic excitability and ii) dendritic spine number. In CA1 pyramidal neurons, we found

397   that ISRIB treatment reversed the age-associated increase in the afterhyperpolarization

398   (AHP) amplitude following high frequency (50 Hz) spiking activity to levels found in

399   young mice. AHP is the hyperpolarization of the neuron after an action potential or

400   series of action potentials. The hyperpolarization affects the amount of depolarization

401   needed for subsequent firing thereby influencing intrinsic excitability. An increase of

402   AHP is associated with aging (*30, 63*) and impaired learning in young adult rodents (*64*).

403   We recapitulated these cellular deficits and we demonstrated that inhibition of the ISR

404   can revert the age-induced increase in intrinsic excitability back to young levels.

405

406   Changes in dendritic spine density or structural reorganization of spines are important

407   for synaptic function (*65*) and cognitive processes such as learning and memory (*33,*

408   *34, 66, 67*). In the aging brain there is a reduction in hippocampal spine density that has

409   been suggested to be responsible for the poor memory functions (*12, 31, 32*). A number

410   of age-related molecular processes have been linked to spine loss including disruption

411   in local protein synthesis (*68*). We demonstrated that ISRIB administration alleviated the

412   age-related reductions in hippocampal spine density.

413

414   ISRIB down-regulated several immune response pathways in the hippocampus of old

415   animals, including IFN response genes. The importance of this molecule in age-related

416   decline has been demonstrated: Type I IFN responses are increased with age, IFN-β

417   expression in the brain is associated with cognitive decline, and injection of IFN-β

418 expressing viral vectors into an adult mouse can induce an old phenotype (*20, 36*). Here

419 we found that ISRIB administration reversed age-induced type I IFN responses in the

420 hippocampus suggesting that ISR activation plays a role in this pathway. However, it is

421 still unclear if this is via a direct or indirect effect on inflammatory cells. Several recent

422 publications have identified deleterious roles for T cells in neuronal health or cognitive

423 decline (*21, 69, 70*). Two recent reports found that persistent T cell infiltration in the

424 brain following viral infection leads to synapse loss (*69, 70*). Investigators identified that

425 IFN-γ produced by T cells mediated synapse loss (*69, 70*). Here we find that ISRIB

426 treatment impacted T cell levels both in the brain and periphery. The changes in T cells

427 and IFN responses directly correlated with cognitive performance and, again, were

428 restored by ISRIB to the levels observed in young animals. Whether ISRIB reverses

429 cognitive decline by directly modulating one of the measured processes (neuronal

430 intrinsic excitability, dendritic spine number, IFN response, or T cell numbers) or by

431 impacting a number of them remains to be determined.

432

433 Aging is an inevitable process for all living creatures, improving our understanding of

434 cellular and molecular processes associated with healthy aging can allow for

435 intervention strategies to modulate cognitive decline. Here we demonstrate that

436 pharmacological attenuation of the ISR can alleviate age-related neuronal and immune

437 changes potentially resetting age-induced cognitive decline.

438

439

440

441

442

443

444

445

METHODS

Animals. All experiments were conducted in accordance with National Institutes of Health (NIH) Guide for the Care and Use of Laboratory Animals and approved by the Institutional Animal Care and Use Committee of the University of California, San Francisco (Protocol 170302). Male and female C57B6/J wild-type (WT) mice were received from the National Institute of Aging. Thy-1-YFP-H (in C57 background) males were bred and aged in house. Old animals started experimentation at ~19 months of age and young animals 3-6 months of age. Animal shipments were received at least one week prior to start of experimentation to allow animals to habituation the new surroundings. Mice were group housed in environmentally controlled conditions with reverse light cycle (12:12 h light:dark cycle at 21 ± 1 °C; ~50% humidity) and provided food and water ad libitum. Behavioral analysis was performed during the dark cycle.

Drug Administration. ISRIB solution was made by dissolving 5 mg ISRIB in 2.5 mLs dimethyl sulfoxide (DMSO) (PanReac AppliChem, 191954.1611). The solution was gently heated in a 40 °C water bath and vortexed every 30 s until the solution became clear. Next 1 mL of Tween 80 (Sigma Aldrich, P8074) was added, the solution was gently heated in a 40 °C water bath and vortexed every 30 s until the solution became clear. Next, 10 mL of polyethylene glycol 400 (PEG400) (PanReac AppliChem, 142436.1611) solution was added gently heated in a 40 °C water bath and vortexed every 30 s until the solution became clear. Finally, 36.5 mL of 5% dextrose (Hospira, RL-3040) was added. The solution was kept at room temperature throughout the experiment. Each solution was used for injections up to 7 day maximum. The vehicle solution consisted of the same chemical composition and concentration (DMSO, Tween 80, PEG400 and 5% dextrose). Stock ISRIB solution was at 0.1 mg/ml and injections were at 2.5 mg/kg. Each animal received an intraperitoneal injection of 2.5x their body weight.

Cmp-003 solution was made by dissolving Cmp-003 (donated by Praxis Biotech) in 50% PEG400 (PanReac AppliChem, 142436.1611) and 50% sterile water. The solution was gently heated in a 40 °C water bath and vortexed every 30 s until the solution became clear. Stock Cmp-003 solution was at 0.5 mg/ml and animal injections were at 5.0 mg/kg. Solution was used immediately and made fresh daily.

Behavioral assessment of cognitive functions. For all assays the experimenter(s) were blinded to therapeutic intervention. Prior to behavioral analysis animals were inspected for gross motor impairments. Animals were inspected for whisker loss, limb immobility (included grip strength) and eye occlusions. If animals displayed _any_ of these impairments, they were excluded. Behavioral assessment was recorded and scored using a video tracking and analysis setup (Ethovision XT 8.5, Noldus Information Technology).

Radial Arm Water Maze.
The radial arm water maze (RAWM) was used to test spatial learning and memory in rodents (_27, 42_). The pool is 118.5 cm in diameter with 8 arms, each 41 cm in length, and an escape platform. The escape platform is slightly submerged below the water

level, so it is not visible to the animals. The pool was filled with water that was rendered opaque by adding white paint (Crayola, 54–2128-053). Visual cues are placed around the room such that they were visible to animals exploring the maze. Animals ran 6 trials a day during learning and 3 trials during each memory probe. On both learning and memory days there is a 10-minute inter-trial interval. Animals were trained for 2 days and then tested on memory tests 24 hours and 8 days after training. During a trial, animals were placed in a random arm that did not include the escape platform. Animals were allowed 1 min to locate the escape platform. On successfully finding the platform, animals remained there for 10 s before being returned to their warmed, holding cage. On a failed trial, animals were guided to the escape platform and then returned to their holding cage 10 s later. The escape platform location was the same, whereas the start arm varied between trials.

Animals were injected (intraperitoneal) with either vehicle or ISRIB (2.5 mg/kg) starting the day prior to behavior (**Figure 2A**) and after each of the final trials of the learning days (day 1 and 2) for a total of three doses. No injections were given when memory was tested on days 3 and 10. RAWM data were collected through a video tracking and analysis setup (Ethovision XT 8.5, Noldus Information Technology). The program automatically analyzed the number of entries into non-target arms made per trial. Every three trials were averaged into a block to account for large variability in performance; each learning day thus consisted of 2 blocks, whereas each memory test was one block each. Importantly, in all animal cohorts tested (regardless of age or drug treatment) learning was measured (Significant time effect observed in all Two-way repeated measure ANOVA analysis when groups are analyzed independently).

*Delayed Matching to Place Barnes Maze***.**
Beginning at day 20 animals were tested on DMP using a modified Barnes maze (*27, 44*). The maze consisted of a round table 112 cm in diameter with 40 escape holes arranged in three concentric rings consisting of 8, 16, and 16 holes at 20, 35, and 50 cm from the center of the maze, respectively. An escape tunnel was connected to one of the outer holes. Visual cues were placed around the room such that they were visible to animals on the table. Bright overhead lighting and a loud tone (2 KHz, 85 db) were used as aversive stimuli to motivate animals to locate the escape tunnel. The assay was performed for 4 days (days 20-23). The escape tunnel location was moved for each day and animals ran four trials on the first two days and 3 trials on the last two days. During a trial, animals were placed onto the center of the table covered by an opaque plastic box so they were not exposed to the environment. After they had been placed on the table for 10 s, the plastic box was removed and the tone started playing, marking the start of the trial. Animals were given 90 s to explore the maze and locate the escape tunnel. When the animals successfully located and entered the escape tunnel, the tone was stopped. If the animals failed to find the escape tunnel after 90 s, they were guided to the escape tunnel before the tone was stopped. Animals remained in the escape tunnel for 10 s before being returned to their home cage. The maze was cleaned with ethanol between each trial. A new escape tunnel was used for each trial. The experimenter was blind to the treatment groups during the behavioral assay. Each trial was recorded using a video tracking and analysis setup (Ethovision XT 8.5, Noldus

538   Information Technology) and the program automatically analyzed the amount of time
539   required to locate the escape tunnel. Animal improvement was calculated by Day 20
540   escape latency – Day 23 escape latency.

541

542   <u>Tissue collection</u>. All mice were lethally overdosed using a mixture of ketamine (10
543   mg/ml) and xylaxine (1 mg/ml). Once animals were completely anesthetized, blood was
544   extracted by cardiac puncture and animals were perfused with 1X phosphate buffer
545   solution, pH 7.4 (Gibco, Big Cabin, OK, -70011-044) until the livers were clear (~1–2
546   min). For Western blot analysis following phosphate buffered solution (PBS), the whole
547   brain (regions dissected discussed below) was rapidly removed and snap frozen on dry
548   ice and stored at −80 °C until processing.

549   <u>Western Blot Analysis</u>. Animals received all 3 ISRIB injections and were terminated 20 h
550   after the third injection (as described above). Frozen brain lysates or hippocampi
551   isolates were then homogenized with a T 10 basic ULTRA-TURRAX (IKa) in ice-cold
552   buffer lysis (Cell Signaling 9803) and protease and phosphatase inhibitors (Roche).
553   Lysates were sonicated for 3 min and centrifuged at 13,000 rpm for 20 min at 4°C.
554   Protein concentration in supernatants was determined using BCA Protein Assay Kit
555   (Pierce). Equal amount of proteins was loaded on SDS-PAGE gels. Proteins were
556   transferred onto 0.2 μm PVDF membranes (BioRad) and probed with primary antibodies
557   diluted in Tris-buffered saline supplemented with 0.1% Tween 20 and 3% bovine serum
558   albumin.

559

560   ATF4 (11815) (Cell Signaling), p-GCN2 (Abcam Cat No ab-75836), p-PERK (Cell Signaling
561   Cat No 3179), p-PKR (Abcam Cat No ab-32036), and p-eIF2 (Cell Signaling, Cat No 3597)
562   and β-actin (Sigma-Aldrich) antibodies were used as primary antibodies. HRP-
563   conjugated secondary antibodies (Rockland) were employed to detect immune-reactive
564   bands using enhanced chemiluminescence (ECL Western Blotting Substrate, Pierce)
565   according to the manufacturer instructions. Quantification of protein bands was done by
566   densitometry using ImageJ software.

567

568   ATF4, p-GCN2, p-PERK, p-PKR and p-eIF2 levels were normalized to β-actin
569   expression and fold-change was calculated as the levels relative to the expression in
570   vehicle-treated derived samples, which corresponds to 1.

571

572   <u>Electrophysiology</u>.
573   Sagittal brain slices (250 μm) including the hippocampus were prepared from old mice
574   (~19 mo) treated with either vehicle or ISRIB or young mice (~3 mo), treated with
575   vehicle, 12-18 hours prior (n = 5, 7, and 5 per group respectively). Mice were
576   anesthetized with Euthasol (0.1 ml / 25 g, Virbac, Fort Worth, TX, NDC-051311-050-01),
577   and transcardially perfused with an ice-cold sucrose cutting solution containing (in mM):
578   210 sucrose, 1.25 NaH_2PO_4, 25 $NaHCO_3$, 2.5 KCl, 0.5 $CaCl_2$, 7 $MgCl_2$, 7 dextrose, 1.3
579   ascorbic acid, 3 sodium pyruvate (bubbled with 95% O_2 − 5% CO_2, pH 7.4) (see Figure
580   3 - **Source Data 1** for reagent information). Mice were then decapitated and the brain
581   was isolated in the same sucrose solution and cut on a slicing vibratome (Leica,
582   VT1200S, Leica Microsystems, Wetzlar, Germany). Slices were incubated in a holding
583   solution (composed of (in mM): 125 NaCl, 2.5 KCl, 1.25 NaH_2PO_4, 25 $NaHCO_3$, 2

584   CaCl$_2$, 2 MgCl$_2$, 10 dextrose, 1.3 ascorbic acid, 3 sodium pyruvate, bubbled with 95%
585   O$_2$ − 5% CO$_2$, pH 7.4) at 36 °C for 30 min and then at room temperature for at least 30
586   min until recording.
587
588   Whole cell recordings were obtained from these slices in a submersion chamber with a
589   heated (32 – 34 °C) artificial cerebrospinal fluid (aCSF) containing (in mM): 125 NaCl, 3
590   KCl, 1.25 NaH$_2$PO$_4$, 25 NaHCO$_3$, 2 CaCl$_2$, 1 MgCl$_2$, 10 dextrose (bubbled with 95% O$_2$ -
591   5% CO$_2$, pH 7.4). Patch pipettes (3–6 MΩ) were manufactured from filamented
592   borosilicate glass capillaries (Sutter Instruments, Novato, CA, BF100-58-10) and filled
593   with an intracellular solution containing (in mM): 135 KGluconate, 5 KCl, 10 HEPES, 4
594   NaCl, 4 MgATP, 0.3 Na$_3$GTP, 7 2K-phosphcreatine, and 1-2% biocytin. CA1 pyramidal
595   neurons were identified using infrared microscopy with a 40x water-immersion objective
596   (Olympus, Burlingame, CA). Recordings were made using a Multiclamp 700B
597   (Molecular Devices, San Jose, CA) amplifier, which was connected to the computer with
598   a Digidata 1440A ADC (Molecular Devices, San Jose, CA), and recorded at a sampling
599   rate of 20 kHz with pClamp software (Molecular Devices, San Jose, CA). We did not
600   correct for the junction potential, but access resistance and pipette capacitance were
601   appropriately compensated before each recording.
602
603   The passive membrane and active action potential spiking characteristics were
604   assessed by injection of a series of hyperpolarizing and depolarizing current steps with
605   a duration of 250 ms from −250 pA to 700 nA (in increments of 50 pA). The resting
606   membrane potential was the measured voltage of the cell 5 min after obtaining whole
607   cell configuration without current injection. A holding current was then applied to
608   maintain the neuron at -67 +/- 2 mV before/after current injections. The input resistance
609   was determined from the steady-state voltage reached during the -50 pA current
610   injection. The membrane time constant was the time required to reach 63% of the
611   maximum change in voltage for the -50 pA current injection. Action potential parameters
612   including the half width, threshold, and amplitude were quantified from the first action
613   potential elicited. Action potential times were detected by recording the time at which
614   the positive slope of the membrane potential crossed 0 mV. From the action potential
615   times, the instantaneous frequency for each action potential was determined (1 / inter
616   spike interval). The maximum firing frequency was the highest frequency of firing
617   identified throughout all current injections. Action potential rate as a function of current
618   injection was examined by plotting the first instantaneous action potential frequency
619   versus current injection amplitude. The F/I slope was then determined from the best
620   linear fit of the positive values of this plot. The action potential or spike threshold was
621   defined as the voltage at which the third derivative of V (d3V/dt) was maximal just prior
622   to the action potential peak. The action potential (AP) amplitude was calculated by
623   measuring the voltage difference between the peak voltage of the action potential and
624   the spike threshold. The half-width of the action potential was determined as the
625   duration of the action potential at half the amplitude. The adaptation index of each cell
626   was the ratio of the last over the first instantaneous firing frequency, calculated at 250
627   pA above the current step that first elicited spiking. The afterhyperpolarization (AHP)
628   was calculated as the change in voltage from baseline (measured as the mean voltage
629   over a 100 ms interval 600 ms after termination of a current injection that first elicited at

least 12 spikes corresponding to a firing frequency of ~50 Hz) compared to immediately after cessation of current injection (the minimum voltage reached in the first 175 ms immediately after cessation of current injection). Cells were excluded from analysis if excessive synaptic input was noted during recording of the mAHP or if the cell did not fire at least 12 spikes during current injections.

To measure the spontaneous excitatory postsynaptic currents (sEPSCs), cells were recorded in voltage clamp at a holding potential of -75 mV for 4 min, a holding potential that should have little inhibitory components given the reversal potential of chloride with these solutions. Analysis of sEPSCs was performed using a template matching algorithm in ClampFit 10.7 (Molecular Devices, San Jose, CA). The template was created using recordings from multiple pyramidal cells and included several hundred synaptic events. Access resistance (Ra) was monitored during recordings, and recordings were terminated if Ra exceeded 30 megaohms. Only stable recordings (< 50 pA baseline change) with a low baseline noise (< 8 pA root mean square) were included. The first 250 synaptic events or all the events measured in the 4 min interval from each cell were included for analysis.

Fluorescent spine imaging preparation. For fluorescent spine analysis, following PBS animals were perfused with ice-cold 4% paraformaldehyde, pH 7.5 (PFA, Sigma Aldrich, St. Louis, MO, 441244) and fixed for 4 - 24 h followed by sucrose (Fisher Science Education, Nazareth, PA, S25590A) protection (15% to 30%). Brains were embedded with 30% sucrose/ Optimal Cutting Temperature Compound (Tissue Tek, Radnor, PA, 4583) mixture on dry ice and stored at -80 °C. Brains were sectioned into 20 µm slides using a Leica cryostat (Leica Microsystems, Wetzlar, Germany) and mounted on slides (ThermoFisher Scientific, South San Francisco, CA). Slides were brought to room temperature (20 °C) prior to use. Tissues were fixed using ProLong Gold (Invitrogen, Carlsbad, CA, P36930) and a standard slide cover sealed with nail polish.

Spine density quantification. For spine density quantification, whole brains from young and old male Thy1-YFP-H transgenic line were used. 3-6 images separated by 60-140 µm in the dorsal hippocampus were imaged per animal and used for dendritic spine density analysis. 9.3 µm z-stack images were acquired on a Zeiss Laser-Scanning Confocal microscope (Zeiss LSM 780 NLO FLIM) at the HDFCCC Laboratory for Cell Analysis Shared Resource Facility. 63x magnification with a water immersion objective. All protrusions from the dendrites were manually counted as spines regardless of morphology. Two individuals (blinded to age and treatment) analyzed a total length of at least 3200 µm of dendrites from each animal using NIH FIJI analysis software (v1.52n). Individual dendritic spine was calculated as density per micron and graphed relative to old mice.

qPCR Analysis. Hippocampus samples, of approximately the same size per animal were process as previously described (*71, 72*). Relative gene expression was determined using the $2^{-\Delta\Delta Ct}$ method and normalized using GAPDH. Primers used were the following:

Cd3: Fw 5' TGACCTCATCGCAACTCTGCTC-3' Rev 5' TCAGCAGTGCTTGAACCTCAGC-3'

Ifit1: Fw 5' CTGAGATGTCACTTCACATGGAA-3' Rev 5' GTGCATCCCCAATGGGTTCT-3'

Rtp4: Fw 5' TGGGAGCAGACATTTCAAGAAC-3', Rev 5'ACCTGAGCAGAGGTCCAACTT-3'

Gbp10: Fw 5' GGAGGCTCAAGAGAAAAGTCACA-3', Rev 5' AAGGAAAGCCTTTTGATCCTTCAGC-3'

Ccl2: Fw 5' GCTGACCCCAAGAAGGAATG-3' Rev 5' GTGCTTGAGGTGGTTGTGGA-3'

Il1β: Fw 5' TGTAATGAAAGACGGCACACC-3' Rev 5' TCTTCTTTGGGTATTGCTTGG-3'

Tnfα: Fw 5' TGCCTATGTCTCAGCCTCTTC-3' Rev 5' GAGGCCATTTGGGAACTTCT-3'

Il-6: Fw 5' TACCACTTCACAAGTCGGAGGC-3' Rev 5' CTGCAAGTGCATCATCGTTGTTC-3'

Irf7: Fw 5'- GAGACTGGCTATTGGGGGAG-3' Rev 5'- GACCGAAATGCTTCCAGGG-3'

Ifitm3: Fw 5'- CCCCCAAACTACGAAAGAATCA-3' Rev 5'- ACCATCTTCCGATCCCTAGAC-3'

Isg15: Fw 5'- GGTGTCCGTGACTAACTCCAT-3' Rev 5'- TGGAAAGGGTAAGACCGTCCT-3'

Ifi204: Fw 5'- AGCTGATTCTGGATTGGGCA-3' Rev 5'- GTGATGTTTCTCCTGTTACTTCTGA-3'

Eif2ak2 (Pkr): Fw 5'- CTGGTTCAGGTGTCACCAAAC-3' Rev 5'- ACAACGCTAGAGGATGTTCCG-3'

Cd11b: Fw 5'- CTGAGACTGGAGGCAACCAT- 3' Rev 5' GATATCTCCTTCGCGCAGAC-3'

Il-10: Fw 5'- GCCAAGCCTTATCGGAAATG- 3' Rev 5' CACCCAGGGAATTCAAATGC -3'

Bdnf: Fw 5'- GGCTGACACTTTTGAGCACGT - 3' Rev 5' CTCCAAAGGCACTTGACTGCTG -3'

721 *Ophn1*: Fw 5'- CTTCCAGGACAGCCAACCATTG
722 - 3' Rev 5' CTTAGCACCTGGCTTCTGTTCC -3'
723
724 *Gbs5*: Fw 5'- CTGAACTCAGATTTTGTGCAGGA - 3' Rev 5'
725 CATCGACATAAGTCAGCACCAG -3'
726
727 *Oasl1*: Fw 5'- CAGGAGCTGTACGGCTTCC - 3' Rev 5'
728 CCTACCTTGAGTACCTTGAGCAC -3'
729
730 *Ppp1r15a*: Fw 5'- GGCGGCTCAGATTGTTCAAAGC - 3' Rev 5'
731 CCAGACAGCAAGGAAATGGACTG -3'
732
733 *Gapdh*: Fw 5' AAATGGTGAAGGTCGGTGTG-3' Rev 5' TGAAGGGGTCGTTGATGG-3'
734

735 <u>Flow Cytometric Analysis</u>. To assess circulating cell populations peripheral blood was
736 collected by cardiac puncture and transferred into an EDTA collection tube. Blood was
737 aliquoted into flow cytometry staining tubes and stained with surface antibodies for 30-
738 60 min at room temperature (*73*). Surface antibodies included anti-CD45 (FITC-
739 conjugated; BD Biosciences), Ly-6G (PE-conjugated; BD Biosciences), CD8 (PE-Cy7-
740 conjugated; BD Biosciences), CD4 (APC-conjugated; BD B), and CD11b (APC-Cy7; BD
741 Biosciences). Leukocyte subpopulations were identified as follows: Forward and side
742 scatter was used to exclude debris and doublet populations. Specific T- cell populations
743 were identified as follows: CD4 T-cell subsets were CD4$^+$, CD45$^+$, Ly-6G$^-$, CD8$^-$, CD11b$^-$
744 . CD8 T-cell subsets were CD8$^+$, CD45$^+$, Ly-6G$^-$, CD4$^-$,CD11b$^-$. After surface antibody
745 staining, red blood cells were lysed with RBC lysis (BD Biosciences). Cell population
746 gating occurred as previously described (*73*). (Data were collected on an LSRII (BD)
747 and analyzed with Flowjo™ software (v10, Tree Star Inc.).
748

749 <u>Statistical Analysis</u>. Results were analyzed using Prism software or IBM SPSS
750 Statistics. Individual animals. Individual animal scores represented by dots, lines depict
751 group mean and SEM. Student t-test, one-way ANOVA, two-way repeated measures
752 ANOVA and Pearson R correlations were used (individual statistical tool and post-hoc
753 analysis denoted in Figure Legends). p values of < 0.05 considered as significant.
754 Group outliers were determined (GraphPad Software Outlier Test-Grubb's test) and
755 excluded from analysis. At most a single animal was excluded from each experimental
756 cohort.
757

758 The numbers of mice used was sufficient to result in statistically significant differences
759 using standard power calculations with alpha = 0.05 and a power of 0.8. We used an
760 online tool (http://www.bu.edu/orccommittees/iacuc/policies-and-guidelines/sample-size-
761 calculations/) to calculate power and samples size based on experience with the
762 respective tests, variability of the assays and inter-individual differences within groups.
763 All experiments were randomized and blinded by an independent researcher prior to
764 treatment.
765

Biological replicates are measurements of biologically distinct animals/tissues/cells used to measure biological differences. Technical replicates are repeated measurements of the same animals/tissues/cells.

FIGURE AND TABLE LEGENDS

Figure 1. ISRIB resets the ISR in the brain of old mice. (**A**) Experimental dosing scheme: ISRIB treatment denoted by syringes (3 injections). (**B**) ISRIB treatment reduced ATF4 protein levels chronically 18 days after ISRIB treatment was complete. One-way ANOVA (F = 18.8, p < 0.001); with Tukey post-hoc analysis. (**C**) Modest age-induced increases in p-GCN2 when comparing young and old male mice. One-way ANOVA (F = 6.6, p < 0.05); with Tukey post-hoc analysis. (**D**, **E**) Age and ISRIB administration did not impact p-PERK or p-PKR protein levels. Brain lysates of specific protein levels listed normalized to actin. Young n = 5, Old = 3, Old + ISRIB = 3. Individual animal values represented by dots; lines depict group mean ± SEM. *p < 0.05; ***p < 0.001

Figure 2. Inhibition of the ISR reverses age-induced decline in spatial, working and episodic memory. (**A**) Experimental Design: Old (~19 months) animals underwent behavioral analysis in a radial arm water maze (RAWM) and a delayed matching to place paradigm (DMP). ISRIB or vehicle administration (2.5 mg/kg intraperitoneal) occurred daily during the learning phase of RAWM denoted by syringes (days 0-2). (**B**) ISRIB treatment improved memory one week after administration in male rodents. One-way ANOVA (F = 4.8, p < 0.05); with Tukey post-hoc analysis. Young n = 10; Old n = 23; Old + ISRIB n = 21. (**C**) Age-induced deficits in working and episodic learning and memory restored weeks after ISRIB administration**.** Animals performed the DMP from day 20 – 23. Average of all trials per group for each day. Day 20, 21 = 4 trials/day. Day 22,23 = 3 trials/day. Two-way repeated measures ANOVA reveals a significant difference between groups p < 0.01 (denoted in figure legend) and time effect p < 0.01. *p < 0.05, **p < 0.01. Old n = 18; Old + ISRIB n = 16. Individual animal scores represented by dots; lines depict group mean ± SEM.

Figure 3. ISRIB treatment alleviates age-associated changes in CA1 pyramidal neuron function and structure. (**A**) Left: Image of pipette patched onto CA1 neuron in sagittal slice of hippocampus. Right: Representative traces from hippocampal CA1 pyramidal neurons from old animals treated with either vehicle (light blue) or ISRIB (dark blue) or young animals treated with vehicle (orange) showing the response to a current injection eliciting ~50Hz spiking activity. Spikes are truncated (dashed line), and the AHP is visualized immediately following cessation of current injection (yellow square) and quantified as the change in voltage from baseline (dotted line). (**B**) Age-induced increases in AHP were measured when comparing young and old animals. ISRIB treatment reversed increased AHP to levels indistinguishable from young animals. Animals were injected with ISRIB (2.5 mg/kg) or vehicle intraperitoneal one day prior to recordings. One-way ANOVA (F = 4.461, p < 0.05); with Tukey post-hoc

812   analysis. *p < 0.05. Each neuron is represented with a symbol; lines indicate the mean ±
813   SEM (Neurons: Young males n = 10 (5 animals); Old males n = 12 (5 animals), Old +
814   ISRIB males n = 19 (7 animals) with 1-5 neurons recorded per animal. (**C-E**) Spine
815   density was quantified in the CA1 region of the dorsal hippocampus from young and old
816   Thy1-YFP-H mice. (**C**) Diagram of hippocampal region analyzed. SR = stratum
817   radiatum. (**D**) Representative images from Old and Old + ISRIB mice. (**E**) A decrease in
818   dendritic spine density was measured when comparing old mice to young mice. ISRIB
819   treatment significantly increased spine density levels of old mice when compared to
820   vehicle treated old mice. 63x magnification with a water immersion objective. Young
821   males n = 7 slides (2 animals); Old males + Vehicle n = 12 slides (3 mice); Old males +
822   ISRIB n = 17 slides (4 mice). Individual slide scores (relative to old mice) represented in
823   dots, lines depict group mean ± SEM. One-way ANOVA (F = 18.57, $p < 0.001$) with
824   Tukey post-hoc analysis. **p < 0.01; ***p < 0.001.

826   **Figure 4. Age-induced inflammatory tone is reduced following ISRIB treatment.**
827   Inflammatory genes were investigated in the hippocampus of young and old mice by
828   qPCR analysis. (**A-C**) ISRIB administration reversed age-induced increases in *Rtp4*,
829   *Ifit1*, and *Gbp10*. (**A**) *Rtp4*, One-way ANOVA (F = 12.23, $p < 0.001$) with a Tukey-post
830   analysis. Young males n = 8; Old males n = 7; Old + ISRIB males n = 8. (**B**) *Ifit1*, One-
831   way ANOVA (F = 8.8; $p < 0.01$) with a Tukey-post analysis. Young males n = 8; Old
832   males n = 7; Old + ISRIB males n = 8. (**C**) *Gbp10*, One-way ANOVA (F = F4.2, $p < 0.05$)
833   with a Tukey-post analysis. Young males n = 8; Old males n = 7; Old + ISRIB males n =
834   7. (**D**) *Cd3* gene-expression (a marker for T cells) changes in the hippocampus of young
835   and old animals were measured by qPCR analysis. *Cd3* was significantly increased with
836   age. ISRIB administration returned *Cd3* expression levels to those comparable to young
837   animals. One-way ANOVA (F = 5.2; $p < 0.05$). Tukey-post hoc analysis. Young males n
838   = 8; Old males n = 7; Old + ISRIB males n = 8. (**E**, **F**) Peripheral T cell levels were
839   measured by flow cytometric analysis of whole blood. (**E**) ISRIB treatment reduced
840    $CD8^+$ T cell percentages (of $CD45^+$ cells) in the peripheral blood. Student t-test. Old
841   males n = 7; Old + ISRIB males n = 8. (**F**) $CD4^+$ T cell percentages (of $CD45^+$ cells)
842   were not impacted. Individual animal scores represented by dots; lines depict group
843   mean ± SEM. (**G**) A significant positive correlation was measured between cognitive
844   performance on day 2 of the RAWM (errors) and multiple inflammatory markers (*Cd3*,
845   *Ifit1*, *Rtp4*, *Gbp10*, *Gbp5*, *Oasl1*, *Ccl2*, *Il-6*) . Linear regression was measured by
846   Pearson R correlation, R value denoted with significance. *p < 0.05; **p < 0.01; ***p <
847   0.001.

849   **Figure 5. ISRIB treatment resets age-related ISR activation**. (**A**) A significant
850   negative correlation was measured between cognitive performance on day 2 of the
851   RAWM (errors) and *Ppp1r15a* mRNA expression. Linear regression was measured by
852   Pearson R correlation, R value denoted with significance. (**B**) ISRIB treatment reduced
853   p-eIF2α protein levels. Brain lysates of p-eIF2α protein levels normalized to actin. Old
854   males n = 10; ISRIB males n = 10. Student's t-test. **p < 0.01. Data are means ± SEM.

Table 1. Impact of age and ISRIB on mRNA expression in the hippocampus. Inflammatory, ISR mediators and neuronal health targets were investigated by qPCR analysis of hippocampal lysates after two ISRIB injections. Columns: (i) mRNA targets (ii) Young group mean ± SEM (iii) Old group mean ± SEM (iv) Old + ISRIB group mean ± SEM (v) ANOVA F value (vi) Significant denotation between groups (vii) n/group.

Figure 1 - **Supplemental Figure 1. ISRIB downregulates ATF4 during administration**. The impact of ISRIB on known ISR activation pathways was investigated by Western blot analysis of brain lysates after 3 ISRIB injections. (**A**) Raw western blot data. Each lane represents an individual animal brain extract. (**B**) ISRIB treatment reduced ATF4 protein levels during drug administration. Old males (7) and females (3): Old n = 10; Old + ISRIB n = 10. Student's t-test. *p < 0.05. Individual animal values represented by dots; lines depict group mean ± SEM.

Figure 1 - **Supplemental Figure 2. ISRIB down-regulates the ISR in the brain of old mice**. The impact of ISRIB on known ISR kinases and activation pathways was investigated by Western blot analysis of brain lysates (raw Western blot data) at day 20.(**A**) ATF4 (**B**) p-GCN2, p-PKR, p-PERK. Each lane represents an individual animal brain extract.

Figure 2 - **Supplemental Figure 1. ISR inhibitors relieve age-induced deficits in spatial learning.** RAWM was used to measure age-induced deficits in spatial learning. Animals ran 2 blocks (3 trials/block) on each learning day. (**A**) Old animals performed significantly worse that young animals. Two-way repeated measures ANOVA revealed a significant interaction (p < 0.001). Bonferroni post-hoc to determine differences at various blocks. Old males n = 19, Young males n = 10. *p < 0.05. (**B**) ISRIB or vehicle administration (2.5 mg/kg intraperitoneal) occurred days 0-2. Compared with the old group, ISRIB treated animals made significantly fewer errors over the course of learning. Two-way repeated measures ANOVA reveals a significant difference between groups p < 0.05. Old males n = 19; Old + ISRIB males n = 15. (**C**) No differences were measured between young +/- ISRIB administration. Two-way repeated measures ANOVA revealed no significant differences. Young males n = 10; Young males + ISRIB n = 10 (**D**) Cmp-003 (5 mg/kg intraperitoneal) administration occurred days 0-2. Old mice that received Cmp-003 performed significantly better than old mice that received vehicle. Two-way repeated measures ANOVA revealed a significant group (p < 0.01) and time effect (p < 0.05). Old males n = 9, Old males + Cmp-003 n = 9. **p < 0.01. Data are means ± SEM.

Figure 2 - **Supplemental Figure 2. ISRIB reduces age-induced memory deficits in female mice.** RAWM was used to measure age-induced deficits in learning and memory. ISRIB treatment improved memory one week after administration in female

903 rodents. Student t-test. Old female n = 12; Old female + ISRIB n = 11. * p < 0.05.
904 Individual animal scores represented by dots, lines depict group mean and SEM.
905
906 Figure 3 – **Supplemental Figure 1. Age and ISRIB treatment do not modify other**
907 **passive or active intrinsic membrane properties in CA1 pyramidal neurons.** (**A**)
908 Representative traces from CA1 pyramidal neurons showing the membrane potential
909 response to a 250 pA current injection in neurons from old animals treated with either
910 vehicle (light blue) or ISRIB (dark blue) or young animals treated with vehicle (orange).
911 Quantification of the action potential (AP) including the half width (**B**), amplitude (**C**),
912 and threshold (**D**) did not show significant differences between CA1 pyramidal
913 recordings from old, old + ISRIB-treated, or young mice. Likewise, evaluation of the
914 maximum firing frequency (**E**) or how the frequency of spiking changes over time,
915 quantified by the adaptation index (**F**) or with current injection, quantified by the slope of
916 the relationship of firing frequency versus amplitude of current injection (F/I slope) (**G**)
917 was also not significantly different between groups. Finally, passive membrane
918 properties including the membrane time constant (tau) (**H**), membrane resistance (Rm)
919 (**I**), and the resting membrane potential (**J**) were not significantly altered by age or ISRIB
920 treatment. Each neuron is represented with a symbol; solid lines indicate the mean ±
921 SEM. (One-way ANOVA for all comparisons; Neurons: and Young males n = 12 (5
922 animals); Old males n = 15 (5 animals), Old + ISRIB males n = 22 (7 animals) with 1-5
923 neurons recorded per animal.
924
925 Figure 3 - **Supplemental Figure 2. Age and ISRIB treatment do not affect**
926 **spontaneous excitatory post-synaptic currents (sEPSC) in CA1 pyramidal**
927 **neurons.** (**A**) Representative whole cell voltage-clamp recordings showing sEPSCs
928 from CA1 pyramidal neurons from old animals treated with either vehicle (light blue) or
929 ISRIB (dark blue) or young animals treated with vehicle (orange). Arrows denote
930 synaptic currents. (**B**) The sEPSC amplitude was not significantly difference between
931 groups (one-way ANOVA). (**C**) The sEPSC frequency was unchanged after ISRIB
932 treatment or compared to young mice (Kruskal-Wallis test). The median amplitude or
933 frequency for each neuron is represented with a symbol; solid lines indicate the mean ±
934 SEM. (Neurons: Young males n = 11 (5 animals); Old males n = 15 (5 animals), Old +
935 ISRIB males n = 18 (7 animals) with 1-5 neurons recorded per animal.)
936
937 Figure 3 – **Source Data 1**. **List of Electrophysiology Reagents**. Column 1 – reagent
938 name; Column 2 – Company of purchase; Column 3 – Catalog number.
939
940 Figure 4 - **Supplemental Figure 1. ISRIB administration does not impact glial cell**
941 **activation.** (**A**) ISRIB administration scheme. (**B-G**) Glial cell was quantified in the
942 stratum radiatum of the CA1 region of the dorsal hippocampus from old Thy1-YFP-H
943 mice. GFAP was used to measure astrocyte activity. Representative images for GFAP
944 staining of (**B**) old and (**C**) old + ISRIB mouse. (**D**) No differences in GFAP percent area
945 were measured when comparing old and old + ISRIB animals. Iba-1 was used to
946 measure microglia activity. Representative images for Iba-1 staining of (**E**) old and (**F**)
947 old + ISRIB mouse. (**G**) No differences in Iba-1 percent area were measured when
948 comparing old and old + ISRIB animals. 63x magnification with a water immersion

objective. Old males n = 12 - 19 slides (3 mice); Old males + ISRIB n = 18 - 20 slides (4 mice). Individual slide scores (relative to old mice) represented in dots, lines depict group mean ± SEM.

Figure 5 - **Supplemental Figure 1. ISRIB treatment breaks age-related ISR activation**. The impact of ISRIB on p-eIF2 was investigated by Western blot analysis of brain lysates after 3 ISRIB injections. Raw western blot data. Each lane represents an individual animal brain extract.

Ethics Statement: All experiments were conducted in accordance with National Institutes of Health (NIH) Guide for the Care and Use of Laboratory Animals and approved by the Institutional Animal Care and Use Committee of the University of California, San Francisco (Protocol 170302).

CONFLICT OF INTEREST

SB is an employee of Praxis Biotech. SB, GU and LD work at Fundacion Ciencia & Vida and receive partial funding from Praxis Biotech. P.W. is an inventor on U.S. Patent 9708247 held by the Regents of the University of California that describes ISRIB and its analogs. Rights to the invention have been licensed by UCSF to Calico. P.W. is a

995 consultant for Praxis Biotech LLC and Black Belt TX Limited.
996
997 The authors declare no other competing interests.
998
999

REFERENCES

1. *Cognitive Aging. Progress in Understanding and Opportunities for Action* (2015).
2. S. L. Connelly, L. Hasher, R. T. Zacks, Age and reading: the impact of distraction. *Psychol Aging* **6**, 533-541 (1991).
3. N. D. Anderson, F. I. Craik, M. Naveh-Benjamin, The attentional demands of encoding and retrieval in younger and older adults: 1. Evidence from divided attention costs. *Psychol Aging* **13**, 405-423 (1998).
4. A. F. Kramer, S. Hahn, D. Gopher, Task coordination and aging: explorations of executive control processes in the task switching paradigm. *Acta Psychol (Amst)* **101**, 339-378 (1999).
5. N. J. Cepeda, A. F. Kramer, J. C. Gonzalez de Sather, Changes in executive control across the life span: examination of task-switching performance. *Dev Psychol* **37**, 715-730 (2001).
6. *An Aging Nation: The Older Population in the United States* (2014).
7. A. Chou, K. Krukowski, J. M. Morganti, L. K. Riparip, S. Rosi, Persistent Infiltration and Impaired Response of Peripherally-Derived Monocytes after Traumatic Brain Injury in the Aged Brain. *Int J Mol Sci* **19**, (2018).
8. H. Yousef *et al.*, Aged blood impairs hippocampal neural precursor activity and activates microglia via brain endothelial cell VCAM1. *Nat Med* **25**, 988-1000 (2019).
9. S. A. Villeda *et al.*, The ageing systemic milieu negatively regulates neurogenesis and cognitive function. *Nature* **477**, 90-94 (2011).
10. J. M. Castellano *et al.*, Human umbilical cord plasma proteins revitalize hippocampal function in aged mice. *Nature* **544**, 488-492 (2017).
11. S. A. Villeda *et al.*, Young blood reverses age-related impairments in cognitive function and synaptic plasticity in mice. *Nat Med* **20**, 659-663 (2014).
12. F. T. Cabral-Miranda, G. Martinez, G. Medinas, D. Gerakis, Y. Miedema, T. Duran-Aniotz, C. Ardiles, AO. Gonzalez, C. Sabusap, C. Bermedo-Garcia, F. Adamson, S. Vitangcol, K. Huerta, H. Zhang, X. Nakamura, T. Pablo Sardi, S. Lipton, SA. Kenedy, BK. Cárdenas, JC. Palacios, AG. Plate, L. Henriquez, JP. Hetz, C., Control of mammalian brain aging by the unfolded protein response (UPR). *Biorxiv*, (2020).
13. J. F. Disterhoft, M. M. Oh, Alterations in intrinsic neuronal excitability during normal aging. *Aging Cell* **6**, 327-336 (2007).
14. E. C. McKiernan, D. F. Marrone, CA1 pyramidal cells have diverse biophysical properties, affected by development, experience, and aging. *PeerJ* **5**, e3836 (2017).
15. M. M. Oh, F. A. Oliveira, J. F. Disterhoft, Learning and aging related changes in intrinsic neuronal excitability. *Front Aging Neurosci* **2**, 2 (2010).
16. V. Rizzo, J. Richman, S. V. Puthanveettil, Dissecting mechanisms of brain aging by studying the intrinsic excitability of neurons. *Front Aging Neurosci* **6**, 337 (2014).
17. L. A. Schimanski, C. A. Barnes, Neural Protein Synthesis during Aging: Effects on Plasticity and Memory. *Front Aging Neurosci* **2**, (2010).

1046   18.   V. Azzu, T. G. Valencak, Energy Metabolism and Ageing in the Mouse: A Mini-
1047   Review. *Gerontology* **63**, 327-336 (2017).
1048   19.   C. Franceschi *et al.*, Inflamm-aging. An evolutionary perspective on
1049   immunosenescence. *Ann N Y Acad Sci* **908**, 244-254 (2000).
1050   20.   K. Baruch *et al.*, Aging. Aging-induced type I interferon response at the choroid
1051   plexus negatively affects brain function. *Science* **346**, 89-93 (2014).
1052   21.   B. W. Dulken *et al.*, Single-cell analysis reveals T cell infiltration in old neurogenic
1053   niches. *Nature* **571**, 205-210 (2019).
1054   22.   J. B. Flexner, L. B. Flexner, E. Stellar, G. De La Haba, R. B. Roberts, Inhibition of
1055   protein synthesis in brain and learning and memory following puromycin. *J
1056   Neurochem* **9**, 595-605 (1962).
1057   23.   C. Lopez-Otin, M. A. Blasco, L. Partridge, M. Serrano, G. Kroemer, The
1058   hallmarks of aging. *Cell* **153**, 1194-1217 (2013).
1059   24.   M. C. Ingvar, P. Maeder, L. Sokoloff, C. B. Smith, Effects of ageing on local rates
1060   of cerebral protein synthesis in Sprague-Dawley rats. *Brain* **108 (Pt 1)**, 155-170
1061   (1985).
1062   25.   C. B. Smith, Y. Sun, L. Sokoloff, Effects of aging on regional rates of cerebral
1063   protein synthesis in the Sprague-Dawley rat: examination of the influence of
1064   recycling of amino acids derived from protein degradation into the precursor pool.
1065   *Neurochem Int* **27**, 407-416 (1995).
1066   26.   H. P. Harding *et al.*, An integrated stress response regulates amino acid
1067   metabolism and resistance to oxidative stress. *Mol Cell* **11**, 619-633 (2003).
1068   27.   A. Chou *et al.*, Inhibition of the integrated stress response reverses cognitive
1069   deficits after traumatic brain injury. *Proc Natl Acad Sci U S A* **114**, E6420-E6426
1070   (2017).
1071   28.   K. Krukowski *et al.*, Integrated Stress Response Inhibitor Reverses Sex-
1072   Dependent Behavioral and Cell-Specific Deficits after Mild Repetitive Head
1073   Trauma. *J Neurotrauma*, (2020).
1074   29.   M. Costa-Mattioli, P. Walter, The integrated stress response: From mechanism to
1075   disease. *Science* **368**, (2020).
1076   30.   C. C. Kaczorowski, J. F. Disterhoft, Memory deficits are associated with impaired
1077   ability to modulate neuronal excitability in middle-aged mice. *Learn Mem* **16**, 362-
1078   366 (2009).
1079   31.   O. von Bohlen und Halbach, C. Zacher, P. Gass, K. Unsicker, Age-related
1080   alterations in hippocampal spines and deficiencies in spatial memory in mice. *J
1081   Neurosci Res* **83**, 525-531 (2006).
1082   32.   B. Xu *et al.*, Loss of thin spines and small synapses contributes to defective
1083   hippocampal function in aged mice. *Neurobiol Aging* **71**, 91-104 (2018).
1084   33.   E. B. Bloss *et al.*, Evidence for reduced experience-dependent dendritic spine
1085   plasticity in the aging prefrontal cortex. *J Neurosci* **31**, 7831-7839 (2011).
1086   34.   N. Yasumatsu, M. Matsuzaki, T. Miyazaki, J. Noguchi, H. Kasai, Principles of
1087   long-term dynamics of dendritic spines. *J Neurosci* **28**, 13592-13608 (2008).
1088   35.   U. I. Onat *et al.*, Intercepting the Lipid-Induced Integrated Stress Response
1089   Reduces Atherosclerosis. *J Am Coll Cardiol* **73**, 1149-1169 (2019).
1090   36.   A. Deczkowska *et al.*, Mef2C restrains microglial inflammatory response and is
1091   lost in brain ageing in an IFN-I-dependent manner. *Nat Commun* **8**, 717 (2017).

1092 37. A. G. Hinnebusch, I. P. Ivanov, N. Sonenberg, Translational control by 5'-
1093 untranslated regions of eukaryotic mRNAs. *Science* **352**, 1413-1416 (2016).
1094 38. N. Sonenberg, A. G. Hinnebusch, Regulation of translation initiation in
1095 eukaryotes: mechanisms and biological targets. *Cell* **136**, 731-745 (2009).
1096 39. A. Chen *et al.*, Inducible enhancement of memory storage and synaptic plasticity
1097 in transgenic mice expressing an inhibitor of ATF4 (CREB-2) and C/EBP
1098 proteins. *Neuron* **39**, 655-669 (2003).
1099 40. S. Pasini, C. Corona, J. Liu, L. A. Greene, M. L. Shelanski, Specific
1100 downregulation of hippocampal ATF4 reveals a necessary role in synaptic
1101 plasticity and memory. *Cell Rep* **11**, 183-191 (2015).
1102 41. R. C. Wek, Role of eIF2alpha Kinases in Translational Control and Adaptation to
1103 Cellular Stress. *Cold Spring Harb Perspect Biol* **10**, (2018).
1104 42. J. Alamed, D. M. Wilcock, D. M. Diamond, M. N. Gordon, D. Morgan, Two-day
1105 radial-arm water maze learning and memory task; robust resolution of amyloid-
1106 related memory deficits in transgenic mice. *Nat Protoc* **1**, 1671-1679 (2006).
1107 43. A. M. Horowitz *et al.*, Blood factors transfer beneficial effects of exercise on
1108 neurogenesis and cognition to the aged brain. *Science* **369**, 167-173 (2020).
1109 44. X. Feng, K. Krukowski, T. Jopson, S. Rosi, Delayed-matching-to-place Task in a
1110 Dry Maze to Measure Spatial Working Memory in Mice. *Bio Protoc* **7**, (2017).
1111 45. M. A. Oliveira Pisco A, Schaum N, Karkanias J, Neff NF, Darmanis S, Wyss-
1112 Coray T, Quake SR, A Single Cell Transcriptomic Atlas Characterizes Aging
1113 Tissues in the Mouse. *bioRxiv*, (2020).
1114 46. D. Mrdjen *et al.*, High-Dimensional Single-Cell Mapping of Central Nervous
1115 System Immune Cells Reveals Distinct Myeloid Subsets in Health, Aging, and
1116 Disease. *Immunity* **48**, 599 (2018).
1117 47. M. H. Brush, D. C. Weiser, S. Shenolikar, Growth arrest and DNA damage-
1118 inducible protein PPP1R15A targets protein phosphatase 1 alpha to the
1119 endoplasmic reticulum and promotes dephosphorylation of the alpha subunit of
1120 eukaryotic translation initiation factor 2. *Mol Cell Biol* **23**, 1292-1303 (2003).
1121 48. J. H. Connor, D. C. Weiser, S. Li, J. M. Hallenbeck, S. Shenolikar, Growth arrest
1122 and DNA damage-inducible protein PPP1R15A assembles a novel signaling
1123 complex containing protein phosphatase 1 and inhibitor 1. *Mol Cell Biol* **21**, 6841-
1124 6850 (2001).
1125 49. I. Novoa, H. Zeng, H. P. Harding, D. Ron, Feedback inhibition of the unfolded
1126 protein response by PPP1R15A-mediated dephosphorylation of eIF2alpha. *J Cell
1127 Biol* **153**, 1011-1022 (2001).
1128 50. E. T. Powers, R. I. Morimoto, A. Dillin, J. W. Kelly, W. E. Balch, Biological and
1129 chemical approaches to diseases of proteostasis deficiency. *Annu Rev Biochem*
1130 **78**, 959-991 (2009).
1131 51. C. Hetz, J. M. Axten, J. B. Patterson, Pharmacological targeting of the unfolded
1132 protein response for disease intervention. *Nat Chem Biol* **15**, 764-775 (2019).
1133 52. C. Sidrauski *et al.*, Pharmacological brake-release of mRNA translation
1134 enhances cognitive memory. *Elife* **2**, e00498 (2013).
1135 53. C. Tenkerian *et al.*, mTORC2 Balances AKT Activation and eIF2alpha Serine 51
1136 Phosphorylation to Promote Survival under Stress. *Mol Cancer Res* **13**, 1377-
1137 1388 (2015).

1138 54. R. Cagnetta *et al.*, Noncanonical Modulation of the eIF2 Pathway Controls an
1139   Increase in Local Translation during Neural Wiring. *Mol Cell* **73**, 474-489 e475
1140   (2019).
1141 55. A. E. Koromilas, M(en)TORship lessons on life and death by the integrated
1142   stress response. *Biochim Biophys Acta Gen Subj* **1863**, 644-649 (2019).
1143 56. K. Klann, G. Tascher, C. Munch, Functional Translatome Proteomics Reveal
1144   Converging and Dose-Dependent Regulation by mTORC1 and eIF2alpha. *Mol*
1145   *Cell* **77**, 913-925 e914 (2020).
1146 57. L. K. Smith *et al.*, beta2-microglobulin is a systemic pro-aging factor that impairs
1147   cognitive function and neurogenesis. *Nat Med* **21**, 932-937 (2015).
1148 58. K. B. Casaletto *et al.*, Cognitive aging is not created equally: differentiating
1149   unique cognitive phenotypes in "normal" adults. *Neurobiol Aging* **77**, 13-19
1150   (2019).
1151 59. K. B. Casaletto *et al.*, Sexual dimorphism of physical activity on cognitive aging:
1152   Role of immune functioning. *Brain Behav Immun* **88**, 699-710 (2020).
1153 60. C. R. Jack, Jr. *et al.*, Age, Sex, and APOE epsilon4 Effects on Memory, Brain
1154   Structure, and beta-Amyloid Across the Adult Life Span. *JAMA Neurol* **72**, 511-
1155   519 (2015).
1156 61. E. J. Davis, I. Lobach, D. B. Dubal, Female XX sex chromosomes increase
1157   survival and extend lifespan in aging mice. *Aging Cell* **18**, e12871 (2019).
1158 62. E. J. Davis *et al.*, A second X chromosome contributes to resilience in a mouse
1159   model of Alzheimer's disease. *Sci Transl Med* **12**, (2020).
1160 63. J. C. Gant, M. M. Sama, P. W. Landfield, O. Thibault, Early and simultaneous
1161   emergence of multiple hippocampal biomarkers of aging is mediated by Ca2+-
1162   induced Ca2+ release. *J Neurosci* **26**, 3482-3490 (2006).
1163 64. M. M. Oh, B. M. McKay, J. M. Power, J. F. Disterhoft, Learning-related postburst
1164   afterhyperpolarization reduction in CA1 pyramidal neurons is mediated by protein
1165   kinase A. *Proc Natl Acad Sci U S A* **106**, 1620-1625 (2009).
1166 65. S. K. Ultanir *et al.*, Regulation of spine morphology and spine density by NMDA
1167   receptor signaling in vivo. *Proc Natl Acad Sci U S A* **104**, 19553-19558 (2007).
1168 66. A. C. Frank *et al.*, Hotspots of dendritic spine turnover facilitate clustered spine
1169   addition and learning and memory. *Nat Commun* **9**, 422 (2018).
1170 67. J. Lu, Y. Zuo, Clustered structural and functional plasticity of dendritic spines.
1171   *Brain Res Bull* **129**, 18-22 (2017).
1172 68. M. Tolino, M. Kohrmann, M. A. Kiebler, RNA-binding proteins involved in RNA
1173   localization and their implications in neuronal diseases. *Eur J Neurosci* **35**, 1818-
1174   1836 (2012).
1175 69. C. Garber *et al.*, T cells promote microglia-mediated synaptic elimination and
1176   cognitive dysfunction during recovery from neuropathogenic flaviviruses. *Nat*
1177   *Neurosci* **22**, 1276-1288 (2019).
1178 70. G. Di Liberto *et al.*, Neurons under T Cell Attack Coordinate Phagocyte-Mediated
1179   Synaptic Stripping. *Cell* **175**, 458-471 e419 (2018).
1180 71. K. Krukowski *et al.*, Traumatic Brain Injury in Aged Mice Induces Chronic
1181   Microglia Activation, Synapse Loss, and Complement-Dependent Memory
1182   Deficits. *Int J Mol Sci* **19**, (2018).

1183   72.   K. Krukowski *et al.*, Female mice are protected from space radiation-induced
1184   maladaptive responses. *Brain Behav Immun* **74**, 106-120 (2018).
1185   73.   K. Krukowski, T. Jones, M. Campbell-Beachler, G. Nelson, S. Rosi, Peripheral T
1186   Cells as a Biomarker for Oxygen-Ion-Radiation-Induced Social Impairments.
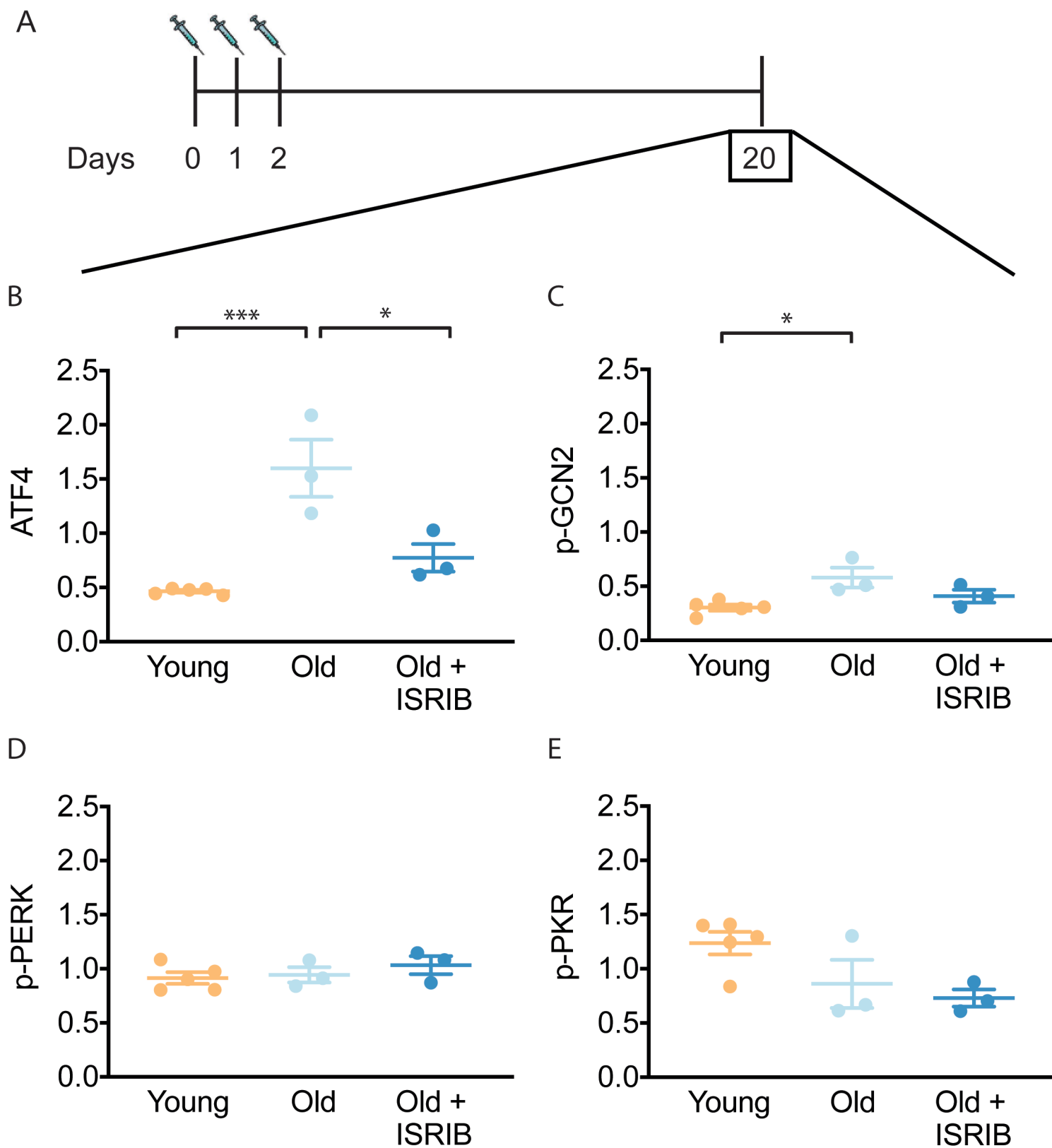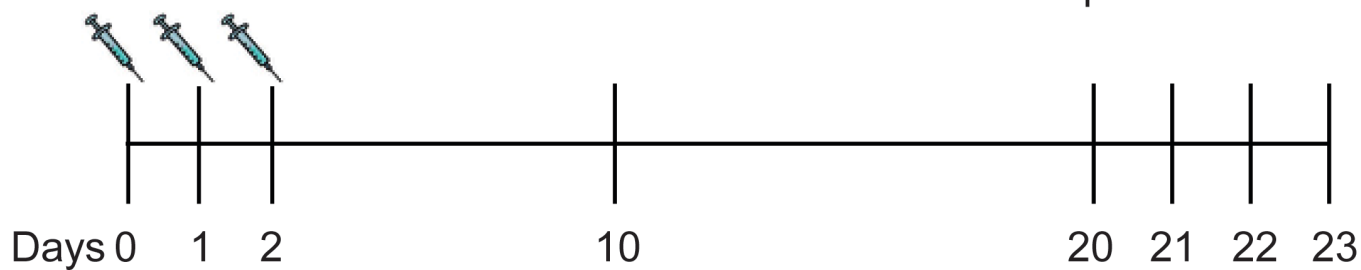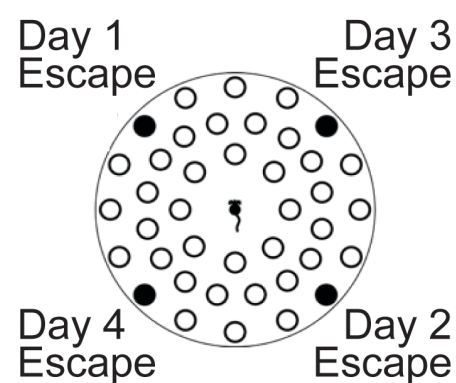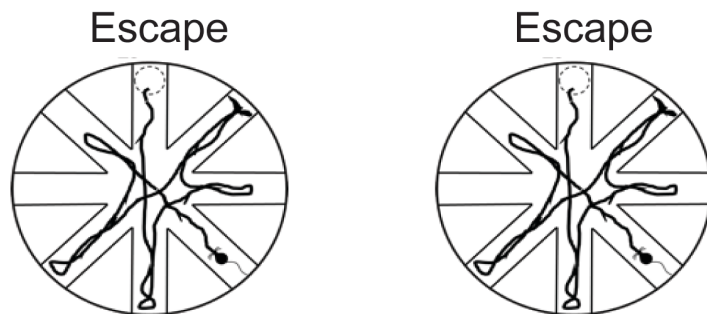1187   *Radiat Res* **190**, 186-193 (2018).
1188

Figure 1

Figure 2

A Radial Arm Water Maze

Escape   Escape

Delayed Matching to Place
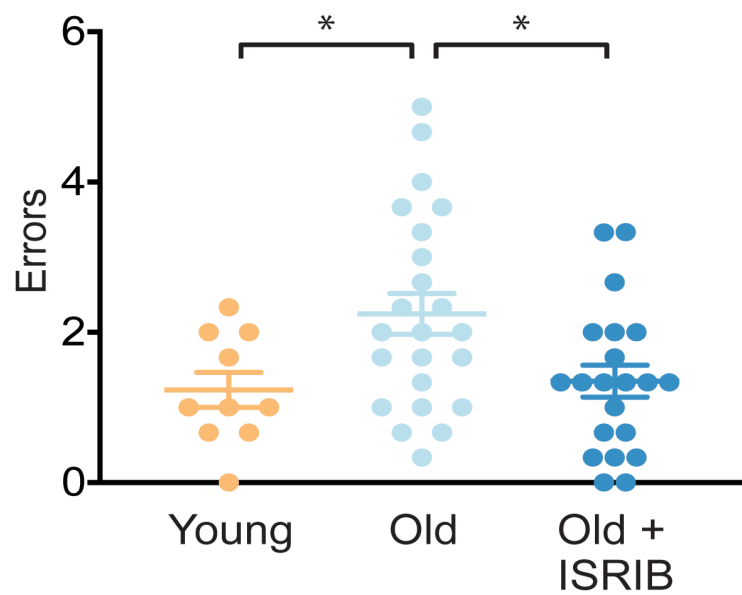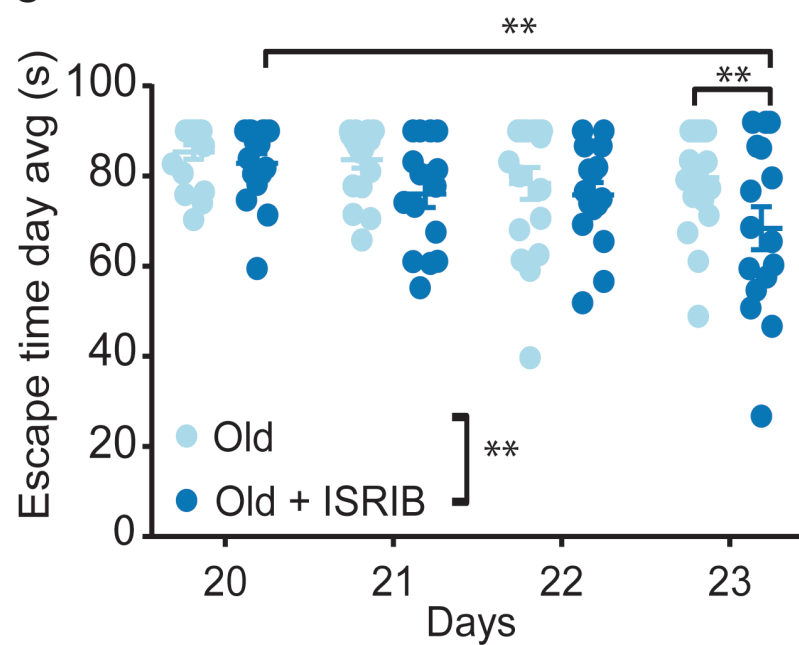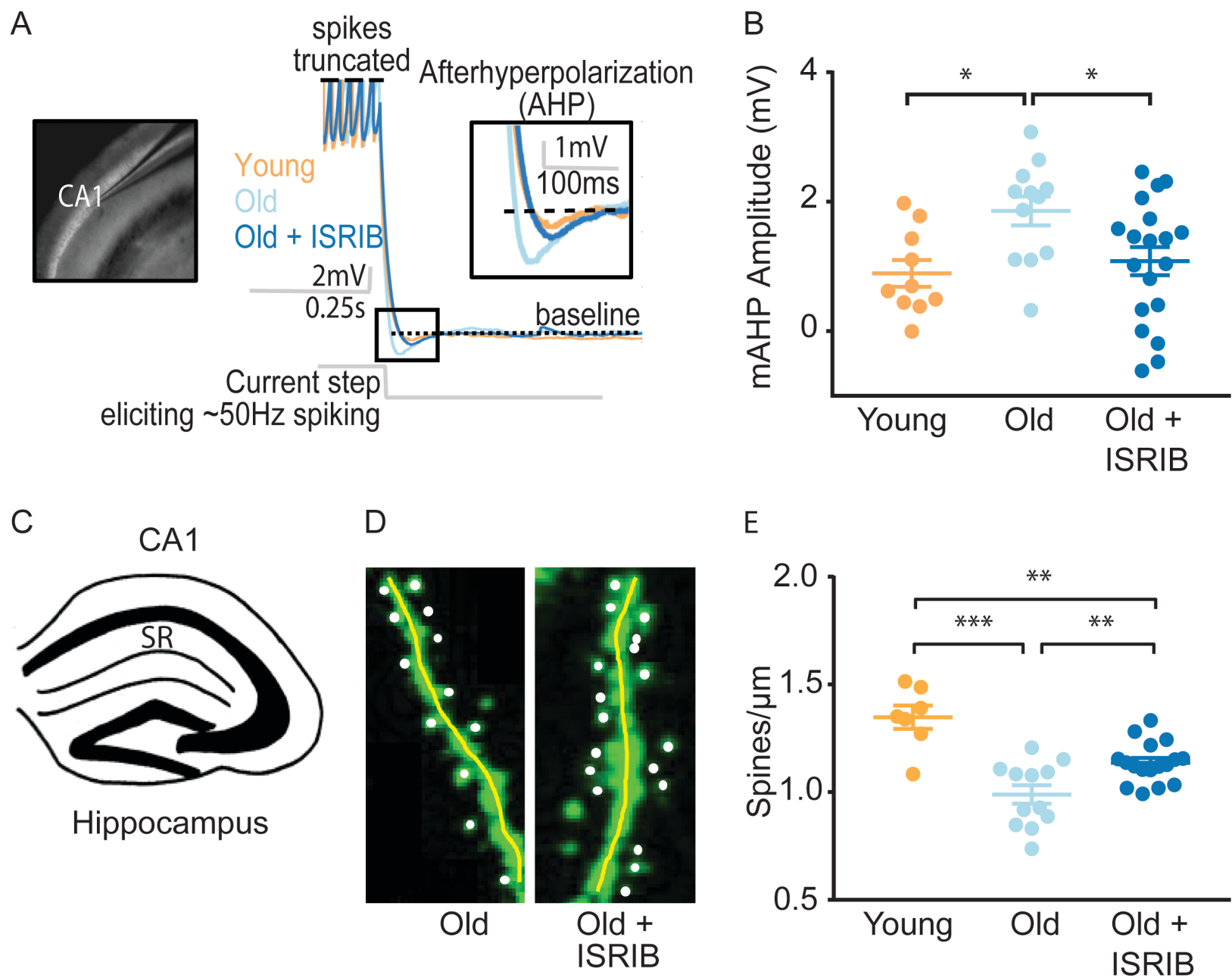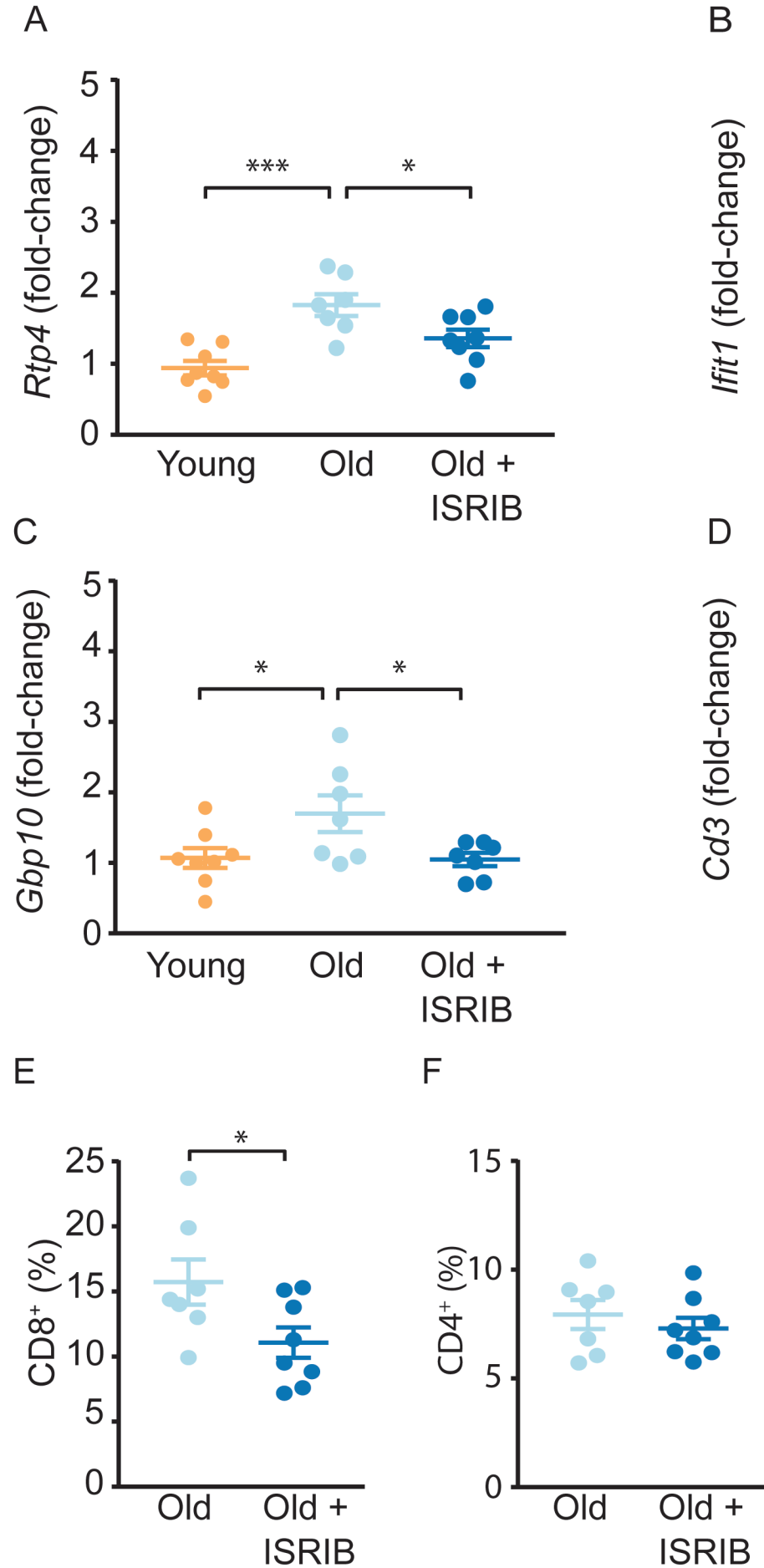
Day 1 Escape   Day 3 Escape

Day 4 Escape   Day 2 Escape

Days 0 1 2   10   20 21 22 23

B

Errors

*

*

Young   Old   Old + ISRIB

C

Escape time day avg (s)

**

**

**

Old
Old + ISRIB

20   21   22   23
Days

Figure 3

A

spikes truncated

Afterhyperpolarization (AHP)

CA1

Young
Old
Old + ISRIB

2mV
0.25s

1mV
100ms

baseline

Current step
eliciting ~50Hz spiking

B

mAHP Amplitude (mV)

*   *

Young   Old   Old +
ISRIB

C

CA1

SR

Hippocampus

D

Old   Old +
ISRIB

E

Spines/µm

**
***   **

Young   Old   Old +
ISRIB

Figure 4

Figure 4

Figure 5

Figure 1 - Supplemental Figure 1

A

Old   Old + ISRIB

38 kDa—   ATF4

42 kDa—   Actin

B

ATF4

1.5

1.0

0.5

0.0

*
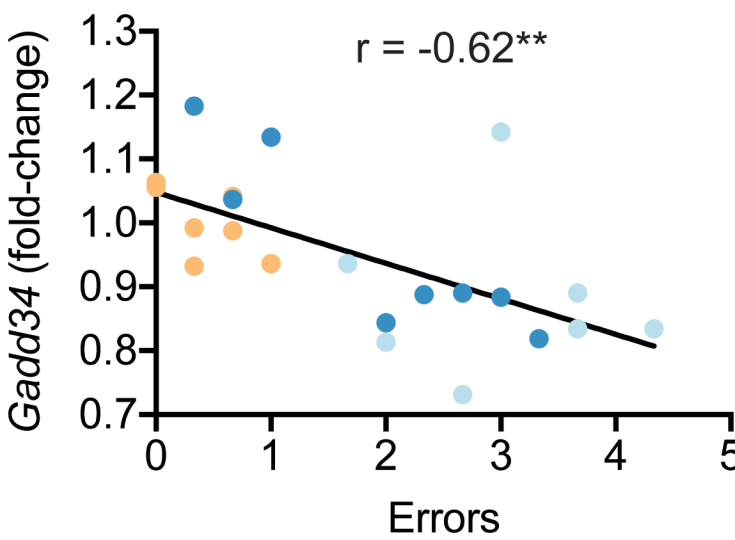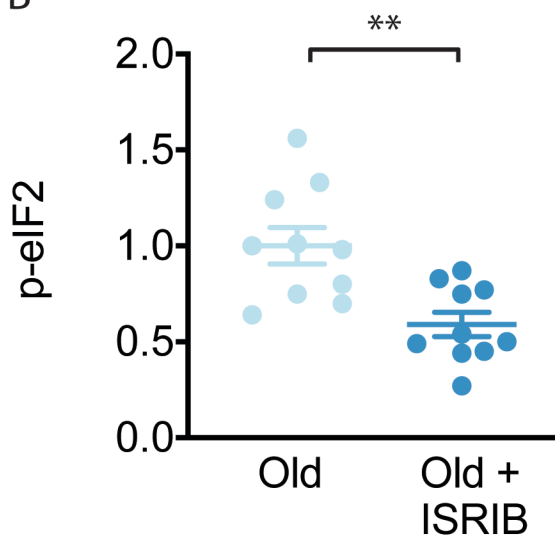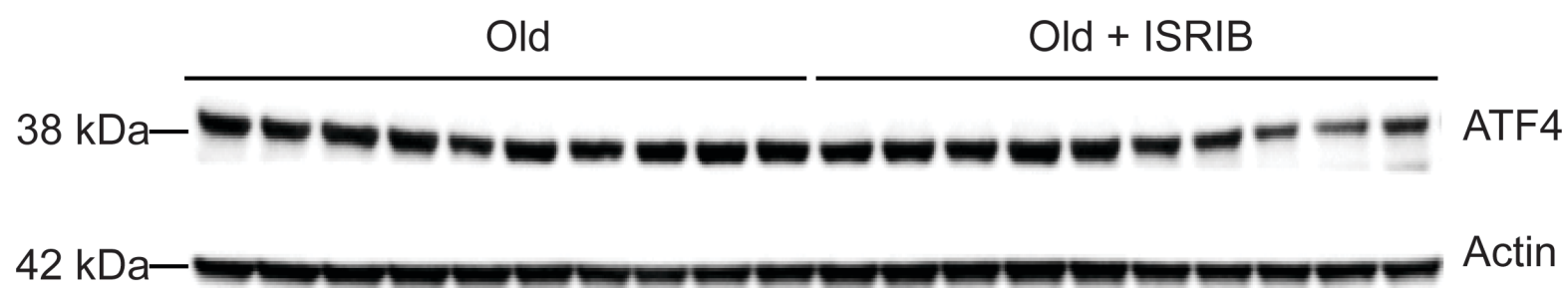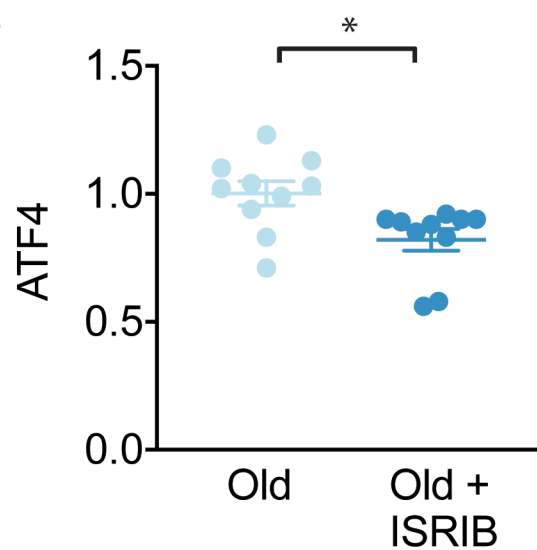
Old   Old +
             ISRIB

Figure 1 - Supplemental Figure 2

A

B
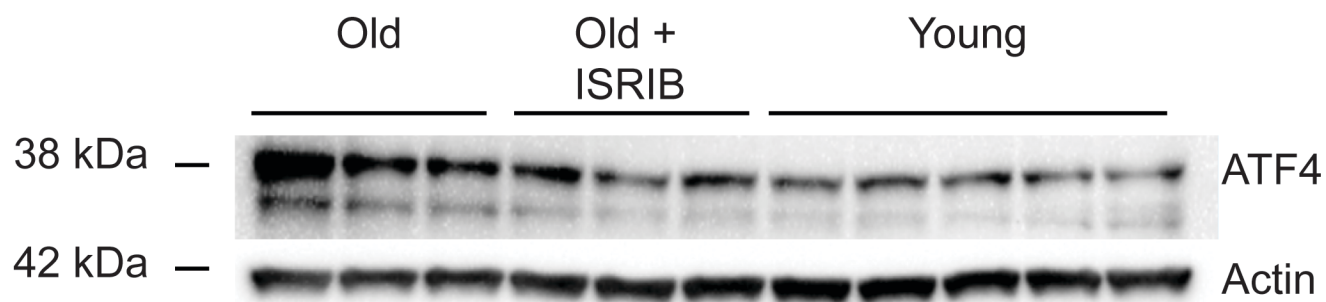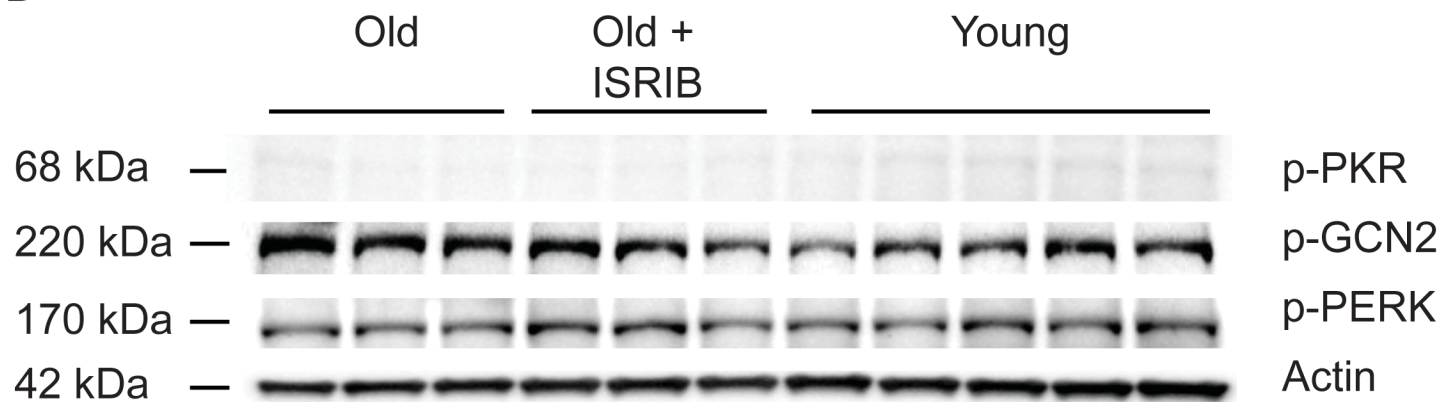
Figure 2 - Supplemental Figure 1
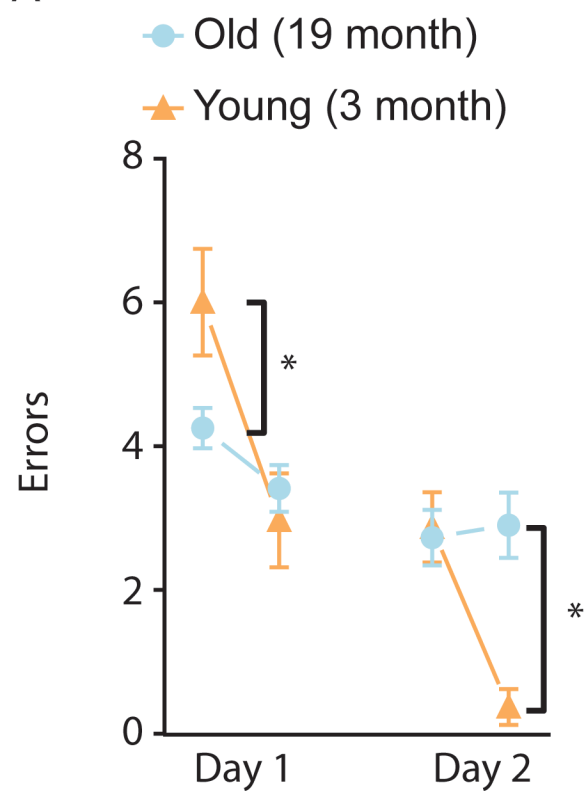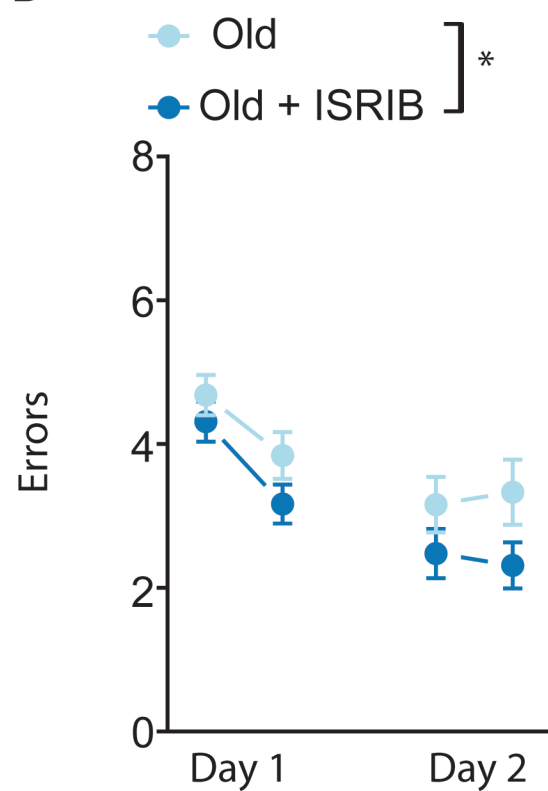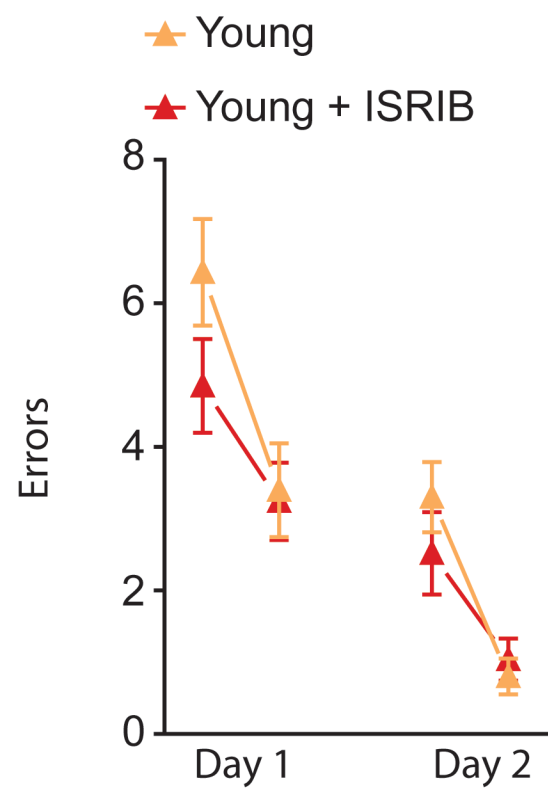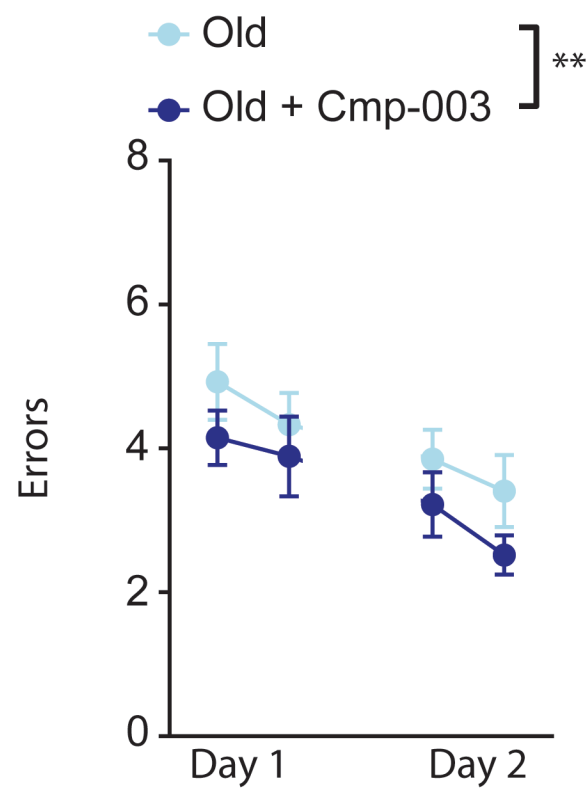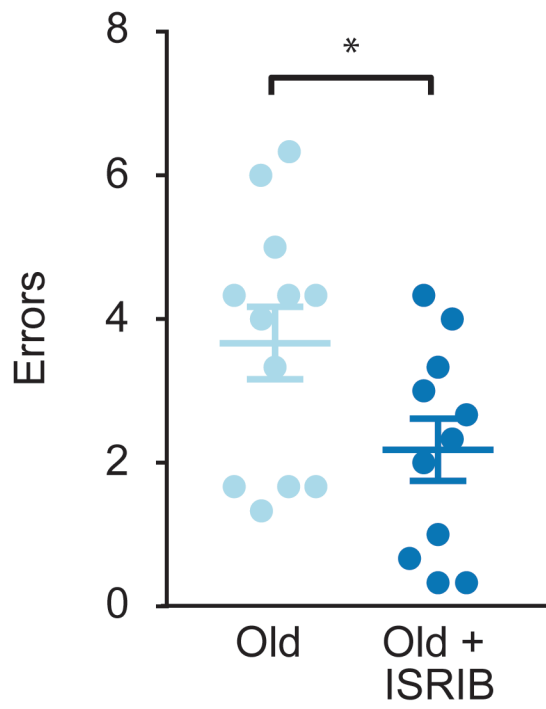
Figure 2 - Supplemental Figure 2

Figure 3 - Supplemental Figure 1
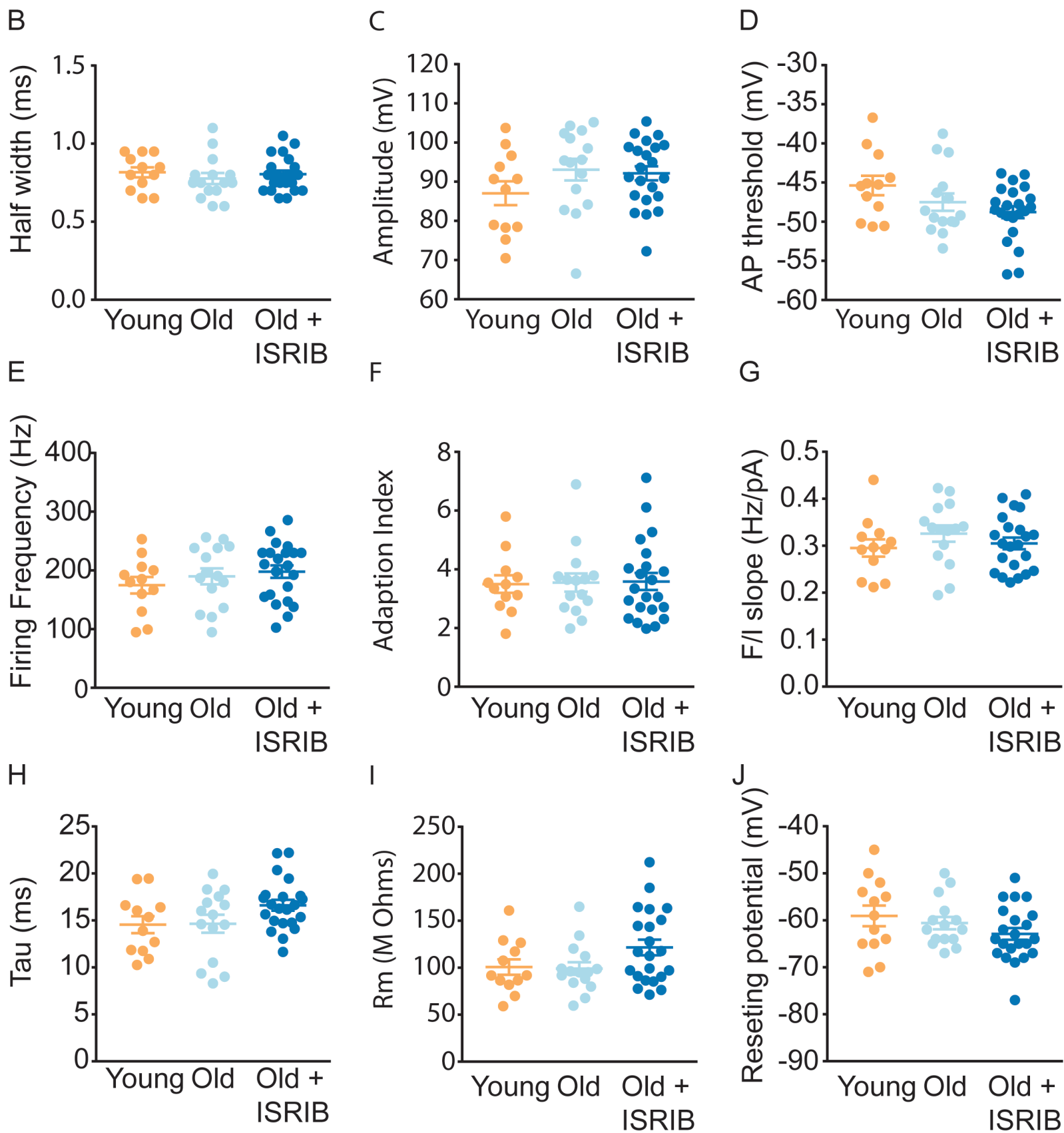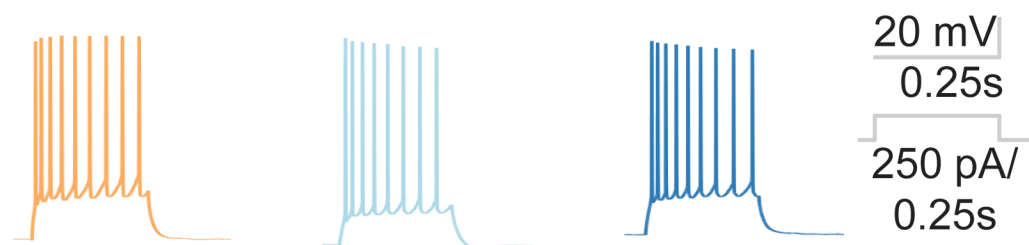
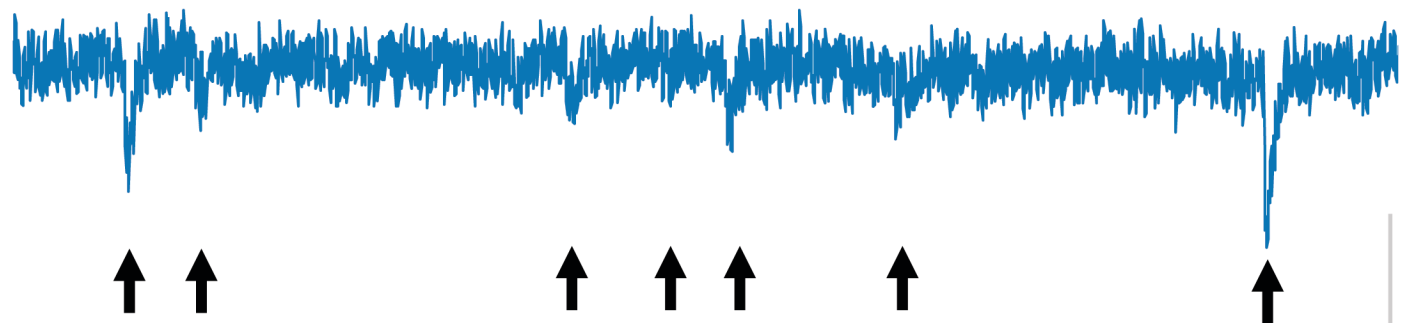# Figure 3 - Supplemental Figure 2
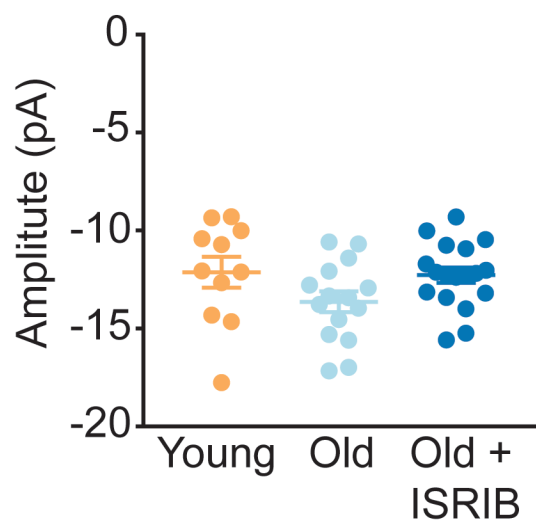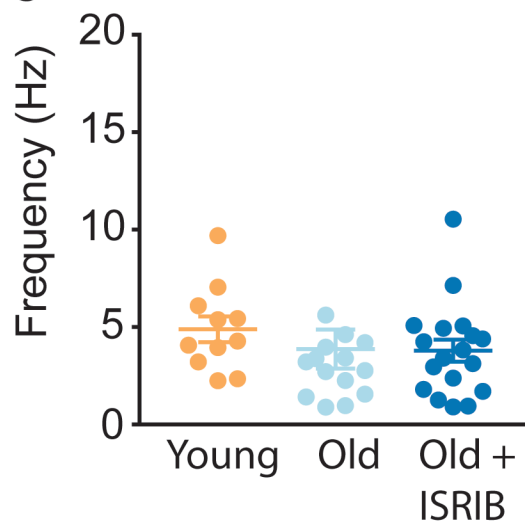
A ↑ = excitatory synaptic current

Young

Old

Old + ISRIB

20 pA

0.4 s

B

Amplitute (pA)

Young   Old   Old + ISRIB

C

Frequency (Hz)

Young   Old   Old + ISRIB

Figure 4 - Supplemental Figure 1
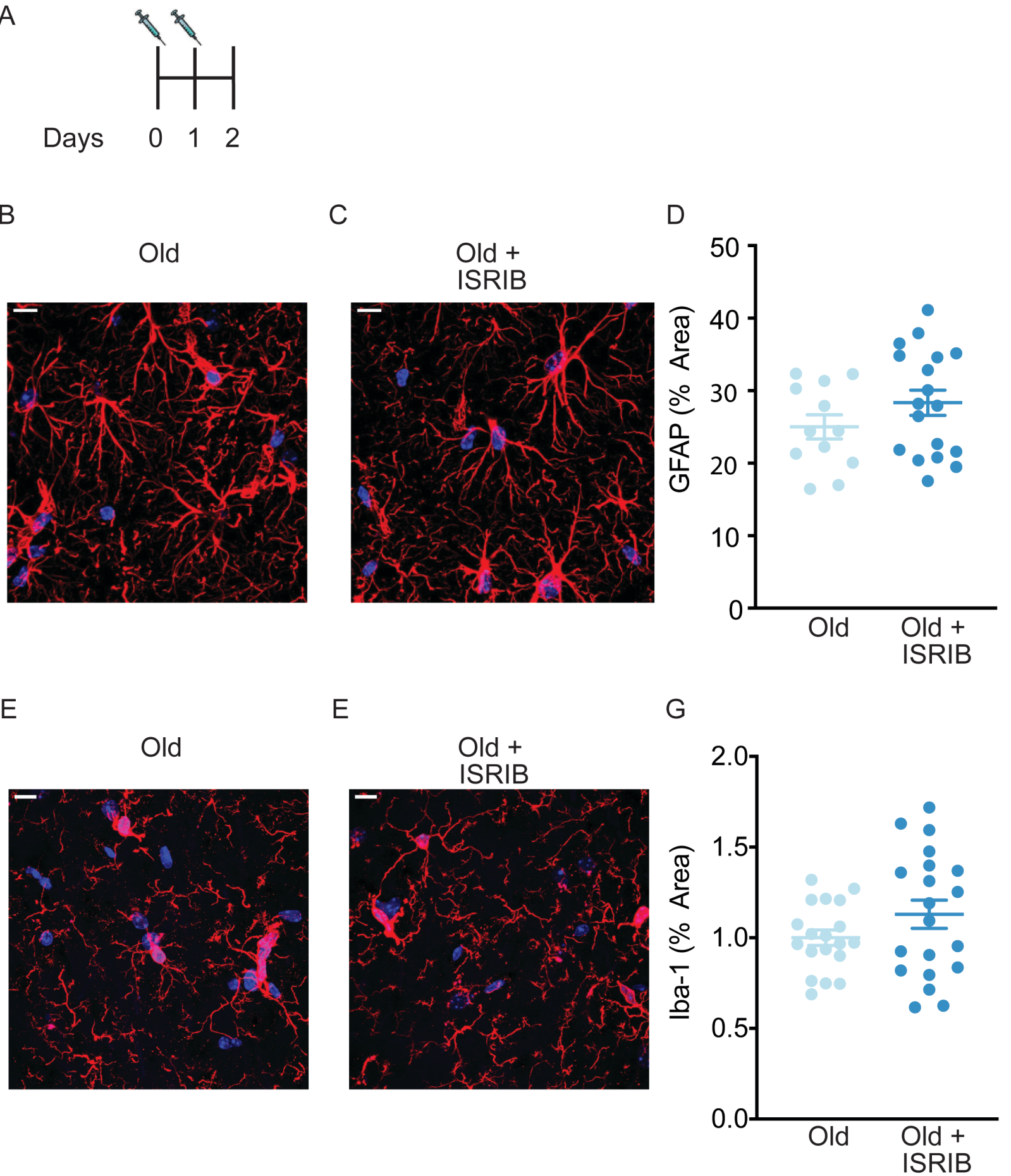
A

Days   0   1   2

B

Old

C

Old +
ISRIB

D

E

Old

E

Old +
ISRIB

G

Figure 5 - Supplemental Figure 1